NASA/TM–2018–220106

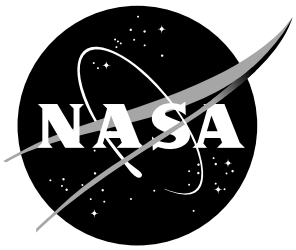

Convergence Analysis of Turbulent Flow Solutions

Harold L. Atkins
NASA Langley Research Center, Hampton Virginia

October 2018

NASA STI Program. . . in Profile

Since its founding, NASA has been dedicated to the advancement of aeronautics and space science. The NASA scientific and technical information (STI) program plays a key part in helping NASA maintain this important role.

The NASA STI Program operates under the auspices of the Agency Chief Information Officer. It collects, organizes, provides for archiving, and disseminates NASA's STI. The NASA STI Program provides access to the NASA Aeronautics and Space Database and its public interface, the NASA Technical Report Server, thus providing one of the largest collection of aeronautical and space science STI in the world. Results are published in both non-NASA channels and by NASA in the NASA STI Report Series, which includes the following report types:

- TECHNICAL PUBLICATION. Reports of completed research or a major significant phase of research that present the results of NASA programs and include extensive data or theoretical analysis. Includes compilations of significant scientific and technical data and information deemed to be of continuing reference value. NASA counterpart of peer-reviewed formal professional papers, but having less stringent limitations on manuscript length and extent of graphic presentations.
- TECHNICAL MEMORANDUM. Scientific and technical findings that are preliminary or of specialized interest, e.g., quick release reports, working papers, and bibliographies that contain minimal annotation. Does not contain extensive analysis.
- CONTRACTOR REPORT. Scientific and technical findings by NASA-sponsored contractors and grantees.
- CONFERENCE PUBLICATION. Collected papers from scientific and technical conferences, symposia, seminars, or other meetings sponsored or co-sponsored by NASA.
- SPECIAL PUBLICATION. Scientific, technical, or historical information from NASA programs, projects, and missions, often concerned with subjects having substantial public interest.
- TECHNICAL TRANSLATION. English-language translations of foreign scientific and technical material pertinent to NASA's mission.

Specialized services also include organizing and publishing research results, distributing specialized research announcements and feeds, providing information desk and personal search support, and enabling data exchange services.

For more information about the NASA STI Program, see the following:

- Access the NASA STI program home page at `http://www.sti.nasa.gov`
- E-mail your question to `help@sti.nasa.gov`
- Phone the NASA STI Information Desk at 757-864-9658
- Write to:
  NASA STI Information Desk
  Mail Stop 148
  NASA Langley Research Center
  Hampton, VA 23681-2199

NASA/TM–2018–220106

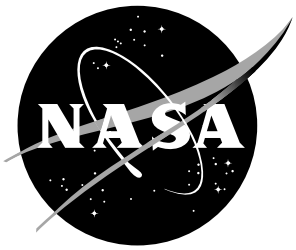

Convergence Analysis of Turbulent Flow Solutions

Harold L. Atkins
NASA Langley Research Center, Hampton Virginia

National Aeronautics and
Space Administration

NASA Langley Research Center
Hampton VA 23681-2199

October 2018

Acknowledgments

This work was performed as part of the Revolutionary Computational Aerosciences discipline under the Transformational Tools and Technologies project of the NASA Transformative Aeronautics Concepts Program.

The use of trademarks or names of manufacturers in this report is for accurate reporting and does not constitute an official endorsement, either expressed or implied, of such products or manufacturers by the National Aeronautics and Space Administration.

Available from:

NASA STI Program / Mail Stop 148
NASA Langley Research Center
Hampton, VA 23681-2199
Fax: 757-864-6500

Abstract

Data from the "Turbulence Modeling Resource" website for turbulent flow over an NACA-0012 airfoil is analyzed to determine the convergence behavior of three second-order CFD codes: CFL3D, FUN3D, and TAU. The convergence of both integrated properties and pointwise data are examined. Several different methods for estimating errors and computing convergence rates are compared. A high-order extension to the Richardson extrapolation is developed that improves the accuracy of the mesh limit values and provides a quantitative estimate of the threshold of the asymptotic regime. The coefficient of total drag exhibits second-order convergence for all three codes, and convergence is monotone over a sequence of 7 grids. Other force coefficients are not so well behaved. The convergence rates of the viscous component of drag on the three finest grids ranges from $\approx$3.0 for CFL3D to $\approx$1.0 for FUN3D. The three codes are converging to similar but not identical solutions. The largest differences between the codes are in the coefficient of lift for which the difference between CFL3D and FUN3D is greater than 10^{-4}. The best agreement occurs in the viscous component of drag, which is the only force component for which all three codes are converging towards each other at a rate of second-order. The agreement between the two unstructured grid codes is good with all properties except lift converging towards common values at a rate of second-order. No one code was universally better than the other. The TAU code has the lowest error in total drag, FUN3D has the lowest error in lift, and CFL3D has the lowest error in the viscous component of drag.

Nomenclature

Variables

R	grid refinement ratio
$S(p, R)$	error scale factor
C_d	coefficient of drag
C_l	coefficient of lift
C_p	coefficient of pressure
C_{d_p}	coefficient of drag due to pressure
C_{d_v}	coefficient of drag due to shear
C_{f_x}	coefficient of friction in x-direction
h	mesh size
p	degree of order property
U	generic solution property
$U(h)$	solution, function of grid size
U_e	exact solution
x	streamwise coordinate direction

Greek

α	error coefficient
Δ_c	difference in property between two codes
Δ_h	difference in property between two grids
Δ_r	difference between property and Richardson extrapolation
$\epsilon(h)$	error, function of grid size
σ	convergence rate

Accents, Supscripts, and Superscripts

$(.)_e$	exact property
$(.)_i$	property on grid-i
$(.)_r$	Richardson extrapolation of a property

1 Introduction

The Turbulence Modeling Resource (TMR) website (ref. 1) provides a large collection of CFD solution data for a variety of test cases that can be used by the turbulence modeling community to verify model implementations within their own codes. The data available at the TMR website has been generated by "previously validated" codes. One test case in particular provides data from three CFD codes for the solution of RANS equations for flow over an NACA–0012 airfoil at a Mach number of 0.15, a Reynolds Number of $6 \cdot 10^6$, and an angle of attack of 10 degrees. The simulations use the Spalart-Allmaras turbulence model, and extensive grid refinement studies are presented as verification that all three codes have successfully implemented that turbulence model. The grid refinement studies make use of several families of consistently and uniformly refined grids. For the current analysis, "Consistent and uniform refinement" means that each coarse grid in the sequence is a subset of the next finer grid produced by retaining the odd-numbered points in each coordinate direction. As such, the data from this case is an excellent resource for a more detailed analysis of the grid convergence of the data. Reference 2 reports on the grid refinement study of this case. The main objective of this article is to provide a more detailed analysis of the convergence behavior of the three CFD codes as applied to this problem. A secondary objective is to demonstrate several methods of evaluating the convergence behavior, examine strengths, weaknesses, and potential pitfalls of the methods.

The three CFD codes that produced the data used in this analysis are CFL3D (refs. 3,4), FUN3D (refs. 5,6), and TAU (ref. 7). The CFL3D and FUN3D codes were developed at the NASA Langley Research Center, and the TAU code was developed by DLR (Deutsches Zentrum für Luft- und Raumfahrt). CFL3D is a structured grid code, whereas FUN3D and TAU are unstructured grid codes. However, the grids used in the simulations are hexahedral-based meshes. All three codes are production codes commonly used for 2D and 3D turbulent flow simulations and are formally second-order accurate. Further, all three codes have previously been shown to produce second order convergence for smooth flows and grids. All three CFD codes use an iterative solution method to solve the RANS equations. It is reported in reference 2 that data produced by FUN3D and TAU codes results from iteratively converging all residuals to machine zero. For data produced by CFL3D, the residual of the continuity equation has been converged to 10^{-13}, the residual of the turbulence model has been converged to 10^{-7}, and aerodynamic force coefficients have converged to 5 significant digits. However, all data files contain data written to 10 significant digits. Reference 2 provides additional references to recent applications of these codes that are relevant to this test case.

Accurate and reliable CFD methods are expected to produce results that have an order property, p, in which the error in the solution, and in most quantities derived from the solution, are expected to behave proportional to h^p in the limit as the mesh size h goes to zero. The error is often modeled simply as

$$\epsilon(h) \equiv U(h) - U_e \approx \alpha h^p \tag{1}$$

in which U_e denotes the exact solution, α is an unknown coefficient, and p is the

order property of the CFD method. The parameters of this model are often determined by fitting data obtained from a grid refinement sequence. There are a number of benefits of knowing (or having estimates of) the parameters of the error model, other than simply estimating error. For example, the cost and resources required to further reduce the error to a particular target level is readily estimated. Many engineering tools for design and optimization rely on gradient-based optimization techniques, which in turn, assume linearizations and Taylor expansions of the solution are sufficiently accurate. Perhaps the oldest practical application of the error model is to provide an estimate of U_e by use of the Richardson extrapolation (ref. 8).

It is important to note that the *exact solution* introduced in equation 1 is the solution to the *continuum mathematical problem* that is approximated discretely by the CFD solver. The processing of validating that a particular CFD solution is a sufficiently accurate representation of a *physical problem* of interest is a separate and independent process. However, it should be clear that validation of the physical accuracy cannot reliably occur if the discretization error is unknown or is known to be poor.

A more realistic but perhaps impractical representation of the error is an infinite polynomial of the form

$$\epsilon(h) \equiv U(h) - U_e \approx \sum_{k=0}^{\infty} \alpha_k h^{p+k} \tag{2}$$

in which the coefficients α_k depend on both the discretization and the solution to the particular problem under consideration. Equations of this form can be derived for the discretization error of simple discretizations and idealized cases (e.g., linear scalar equations, linear discretizations, uniform grids) by evaluating the Taylor expansion of the discrete equations, also called *modified equation analysis* (ref. 9). However, the solution error is not directly proportional to the discretization error, as error may propagate and diffuse through the problem domain in a manner similar to the solution itself. Integrated properties are further subject to cancelation of errors, possibly resulting in an oscillatory convergence pattern. An integrated property may cross the exact (but unknown) value at several points in a grid refinement sequence before settling to an asymptote; while the underlying solution may be converging monotonically over most of the domain. Nonetheless, in realistic complex applications, it is generally assumed that the solution error is of a functional form similar to equation 2, and therefore, that the asymptotic behavior is well modeled by equation 1.

The task of evaluating the convergence properties involves not only determining estimates of error and convergence rates, but equally and perhaps more importantly, determining whether or not a particular grid refinement sequence even includes the asymptotic regime. Attempts to fit the simple error model, equation 1, to a measured error metric using a grid sequence outside of the asymptotic regime can lead to highly inaccurate estimates of the error and convergence rates. The ability to recognize this situation often requires experience and engineering judgement.

The second section analyzes the convergence of integrated force coefficients of lift and drag, and of the viscous and inviscid components of drag (or specifically,

shear-stress and pressure contributions, respectively). The convergence rates, error estimates, and estimates of the limit solution are evaluated by two methods for each force coefficient predicted by each code. The grid convergence of code-to-code comparisons are also presented and analyzed. The Richardson extrapolation is applied to determine limit conditions, and also to provide an enhanced examination of the grid convergence of individual components and of code-to-code comparisons. Finally, a high-order extension to the Richardson extrapolation is introduced to provide enhanced limit conditions and to provide a quantitative measure of the upper threshold of the asymptotic regime.

The third section analyzes the convergence of point values of the pressure coefficient, C_p, and the x component of the shear stress, C_{f_x}, again using two different methods for assessing the error. Code-to-code comparisons of pointwise data are also presented. The fourth section explores the facility of the pointwise convergence analysis to diagnose potential problems with the data.

As the main thrust of this work is to analyze the convergence of data from the TMR website, and standard approaches for convergence analysis are well established in literature (ref. 10 and references therein), a detailed description of the analysis techniques is relegated to an Appendix of this article. However, the Appendix does provide new arguments and evidence regarding the application and interpretation of some of the traditional approaches. The Appendix also provides additional details concerning the high-order extension to the Richardson extrapolation introduced in the third section.

2 Convergence of Integral Properties

Convergence of the coefficients of lift and drag (C_l, C_d, C_{d_p}, and C_{d_v}) are analyzed. The data for this analysis was taken from the following files downloaded on 1/16/2018 from the TMR website:

`cfl3d_results_sa_nopv_2ndorderturbadvection_withN.dat`,

`fun3d_results_sa_nopv_withN.dat` and

`tau_results_sa_nopv_withN.dat`.

Each file contains data for three different grid families, identified as Family I, II or III. This analysis only considers grid Family II, which consists of a sequence of seven grids. The grids are numbered with 0 denoting the finest grid, and each unit increase indicates a 2X coarsening of the grid. Properties associated with a particular grid will be identified by an integer suffix (e.g., h_0 denotes a representative mesh size of the finest grid, $U_n \equiv U(h_n)$, and $C_{l,n}$ denotes C_l on the n-th grid). The files provide data produced by the FUN3D and TAU codes for all seven grids and data produced by CFL3D on the six finest grids.

An increasingly common practice for assessing the convergence of flow properties predicted by 2nd-order CFD codes is to present data as a function of the square of the mesh size. A linear behavior of such plots is taken as confirmation that the CFD code is second order, and that the results are within the asymptotic regime. However, this approach has several deficiencies illustrated in figures 1(a-l). Each row presents a different property, and each column presents the data at a different

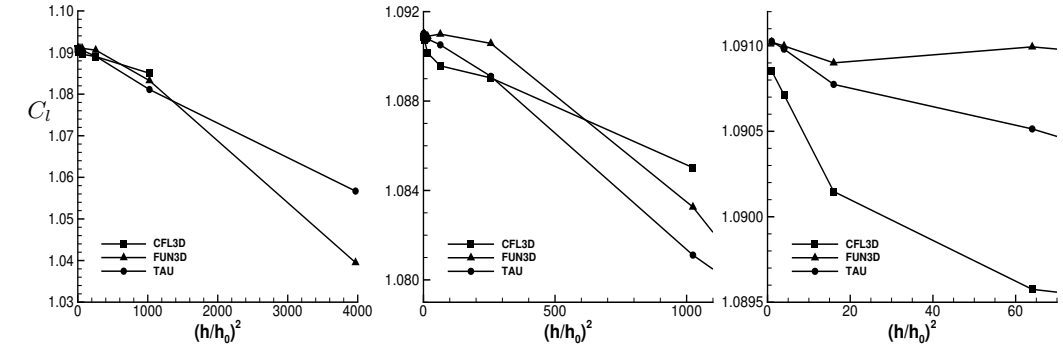

(a) C_l, all grids. (b) C_l, intermediate scale. (c) C_l, four finest grids.

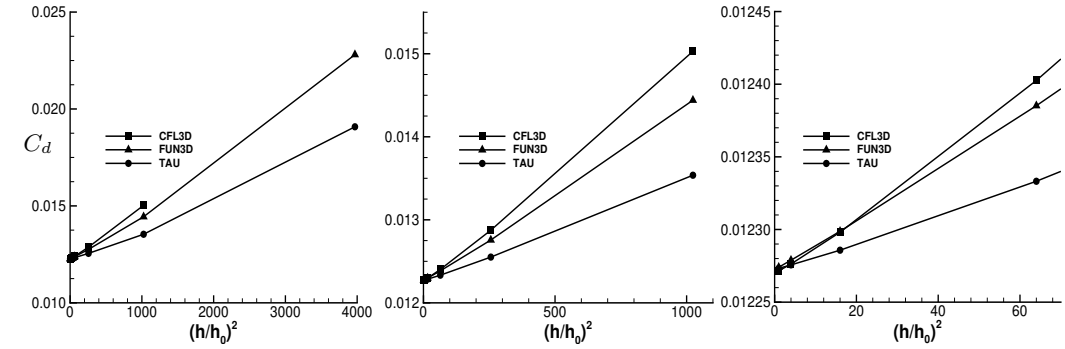

(d) C_d, all grids. (e) C_d, intermediate scale. (f) C_d, four finest grids.

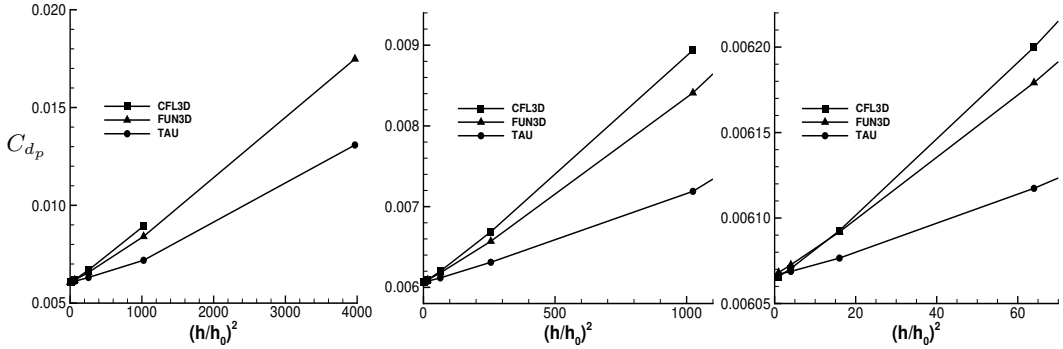

(g) C_{d_p}, all grids. (h) C_{d_p}, intermediate scale. (i) C_{d_p}, four finest grids.

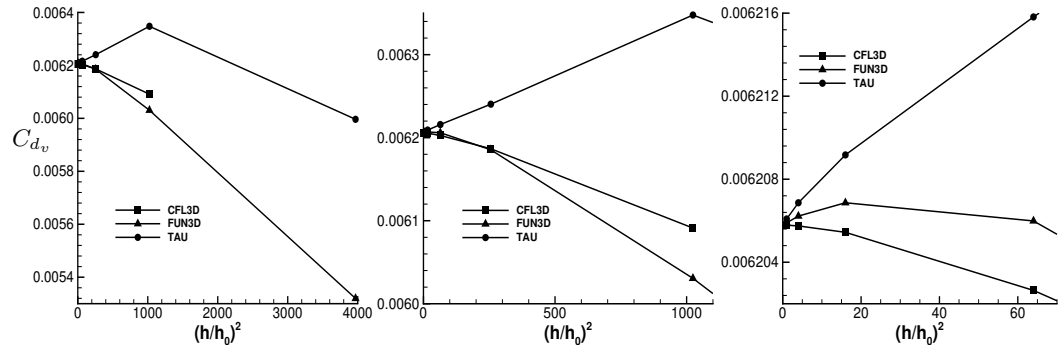

(j) C_{d_v}, all grids. (k) C_{d_v}, intermediate scale. (l) C_{d_v}, four finest grids.

Figure 1. Lift and drag coefficients plotted vs. $(h/h_0)^2$ viewed on multiple scales.

scale. The left column of plots presents a scale that contains all grids, the right column presents a scale that shows only the four finest grids, and the middle column presents an intermediate scale. The first attribute of this approach, apparent in all 12 plots, is that the h^2 behavior clusters the fine grid data toward the origin such that data of only four grids are distinctly discernible at any particular scaling. Consequently, detection of evolving trends requires viewing the data on several scales. The clustering would intensify if such an approach were extended and applied to a high-order method, and any ability to observe a linear trend would be further diminished. Additionally, this approach requires subjective assessment as to how straight is straight enough to declare that a result is essentially second order. This point is well illustrated by C_l and C_{d_v}, for which both the left and middle column plots present data that is somewhat straight for some codes, but only the third column (the finest grids) reveals that they are not so. A concise and quantitative approach that requires less subjective evaluation would be preferable.

The methods used for estimating error are described briefly here, and further details are provided in the Appendix. Throughout this work, Δ_x will be used to denote an error estimate in which the subscript "x" identifies the particular method of estimation. The first method uses the Richardson extrapolation (refs. 8, 11) computed from the two finest grids as a surrogate for the exact solution, U_e, and estimates the error as the difference between the solution and the Richardson extrapolation: $\Delta_r U_i \equiv U_i - U_{r,0}$ in which U denotes any solution property of interest. The Richardson extrapolation is computed as $U_{r,i} = (R_i^p U_i - U_{i+1})/(R_i^p - 1)$ in which $R_i \equiv h_{i+1}/h_i$ is the ratio of mesh sizes.

The second error estimate is simply the difference between a solution property on successive grids, optionally scaled by a function of the design order p (if known), $\Delta_h U_i \equiv S(p, R_{i-1})(U_i - U_{i-1})$. The scaling function $S(p, R)$, derived in the Appendix, shifts the second estimate in a manner that will make it equal to $\Delta_r U_i$ if the data are in the asymptotic regime. The scaling does not affect the slope of the curve or the convergence rate computed from the curve, but serves only to facilitate visual comparisons.

Because all three CFD codes have been previously verified to be second order, the design order of $p = 2$ is used for both the Richardson extrapolation and the scaling function $S(p, R)$. For the current data sets with constant $R = 2$, the Richardson extrapolation becomes $U_{r,i} = (4\,U_i - U_{i+1})/3$, and the scaling becomes the constant $S(p, R) = 4/3$. Contrary to established practices (refs. 10, 12, 13), the Appendix provides arguments for preferring the design order (if known) over the order property computed from the data. Further, the Appendix provides arguments for avoiding the use of any extrapolations if the design order is not known, and a reasonable guess cannot be made. Exact agreement between the two error measures on grid-1 ($h = h_1$) occurs because both methods invoke the same formulas, assumptions, and data about that point (e.g., the simple error model, equation 1, with an assumed order fit to the two finest grids). Also, the slope of Δ_r between the two finest grids will be exactly the order used to compute the Richardson extrapolation. This slope should not necessarily be viewed as indicative or predictive of behavior if the mesh were refined further, although it may be. However, this segment of the curve provides a reference "sight line" by which convergence on coarser grids can be

3 Convergence of Local Properties

Convergence of local pointwise properties C_p and C_{f_x} are analyzed and presented in figures 7 through 10. The data for this analysis was taken from the following files downloaded on 12/6/2017 from the TMR website:

`cfl3d_cp_sa_nopv.dat`, `cfl3d_cf_sa_nopv.dat`,

`fun3d_cp_sa_nopv.dat`, `fun3d_cf_sa_nopv.dat`,

`tau_cp_sa_nopv.dat`, and `tau_cf_sa_nopv.dat`.

The files contain coefficients for only the four finest grids of the grid sequence. It is noted that the data in these files are located at grid nodes, and also that the FUN3D and TAU codes are node-centered finite-volume methods that store the dependent flow variables at the node locations. However, CFL3D is a cell-centered finite-volume method, and the data have been interpolated to the node locations in order to facilitate the comparisons. Thus, the CFL3D results contained in the above files have been subjected to more post processing than either the FUN3D or TAU results. In contrast, the integrated data discussed in the last section were computed by each code using its own internal procedures and presumably was not subject to unnecessary interpolations.

Figure 7 presents pointwise error estimates of C_p and the associated convergence rate as a function of the arc length around the airfoil, s. The error estimate is computed from the difference between C_p on pairs of meshes, $\Delta_h C_{p,i}$. Generally the estimated errors are higher on the upper surface than on the lower surface for all three codes. All three codes have localized peaks in the error estimate near leading and trailing edges. The leading edge peaks, at $s = 0$, are of similar magnitudes for CFL3D and TAU codes, while the leading edge peak for FUN3D is lower. The trailing edge peaks are generally comparable to or lower than the leading edge peaks. Away from these peaks, the error estimates for FUN3D are the lowest of the three codes. Estimated error levels of CFL3D and TAU are similar, with those of the TAU code being slightly lower. The TAU code exhibits the most monotone convergence. The convergence rate computed from the three finest grids is well below design value of 2.0, but the rate is increasing with refinement. The convergence rates of FUN3D and CFL3D computed from the three finest grids is close to the design value of 2.0, however, the two coarser grids exhibit oscillatory convergence and are clearly outside of the asymptotic regime. The CFL3D data appear to be contaminated with numerical noise, but otherwise, it has the most uniform convergence rate with respect to s.

Figure 8 presents an analysis of the same data in which the error is estimated by $\Delta_r C_p$. As with the integral properties examined in the previous section, $\Delta_r C_p \equiv \Delta_h C_p$ on grid-1, because of the common assumptions and formulas shared between the Richardson extrapolation and the scaling function, $S(p, R)$. Also, the drop in error between the two finest grids is exactly 4.0 and the convergence rate is exactly 2.0, due solely to the assumptions made in the Richardson extrapolation. In practice, the convergence rates based on the Richardson extrapolation for the two finest grids should probably not be presented without sufficient caveats so as to avoid misleading a reader into believing that the simulation data are converging at

visually judged.

The formula for the convergence rate, simplified for the current case with constant ratio grid refinement, is the same for both error estimates and is given by

$$\sigma_i = \log\left[\frac{|\Delta U_{i+1}|}{|\Delta U_i|}\right] / \log(2.0) \tag{3}$$

in which Δ without a subscript will be used whenever a formula or a point of discussion applies to any form of error estimate. Note that the computed convergence rate, σ_i, is distinguished from the order property of the simulation method, p, to emphasize that σ_i is the result of a curve fit to data produced by the simulation, whereas p denotes a theoretical property of the simulation method. It is expected that σ_i will approach p in the limit of the mesh size going to zero.

Figure 2 presents quantitative error estimates and convergence rates for lift and drag coefficients. The upper set of curves in each plot shows an estimate of the error computed by the two methods. The lower set of curves gives the corresponding convergence rate. The total drag coefficient and the contribution from pressure, C_d and C_{d_p}, both converge at a constant rate of $\approx$2.0 over the entire grid sequence for all three codes. The estimated errors for CFL3D and FUN3D are similar to each other and larger than that of the TAU code by a factor of two to three. Both methods of estimating the error give essentially the same result.

The uniform convergence characteristics of C_d and C_{d_p} over such a broad range of grid sizes is uncommon. In figures 2a and c, C_l and C_{d_v} exhibit a more typical pattern in which the convergence of the error goes through a transition in which the influence of high-order terms is evident on the coarser grids. The transition can be monotone or oscillatory, and oscillatory transitions will appear differently for the different error estimates. The response of the different error estimates to an oscillatory error is examined more closely in the Appendix Section A.1. The simple error model given by equation 1 is a monotone equation, and any attempt to fit it to a nonmonotone data set is problematic. If the sign of the error estimate changes as the mesh is refined, then obviously the error estimate has passed through zero, and it can take on small values. Small values in either the numerator or the denominator of equation 3 will result in unreasonably low or high values of the convergence rate. In this work, abnormally high or low convergence rates are treated as spurious values and are excluded from the plots.

The error estimates for C_l are the highest of the four coefficients examined. FUN3D has the lowest error estimate for C_l. CFL3D is about an order of magnitude higher and is the highest. Convergence of C_l is oscillatory for all three codes with the transition occurring above grid-2. The transition does not noticeably influence the computation of the convergence rate on grid-1, and all three codes are converging at a rate of $\approx$2.0 on the three finest grids.

The estimated errors in the viscous contribution to drag, C_{d_v}, are the lowest of the four coefficients examined. The estimated error of the CFL3D code is an order of magnitude lower than that of FUN3D and TAU codes. Convergence of C_{d_v} undergoes a transition between grid-1 and grid-4, and the influence of higher-order terms is evident above grid-1. The transition is monotone for CFL3D and TAU codes, and both error estimates give similar results. FUN3D exhibits oscillatory

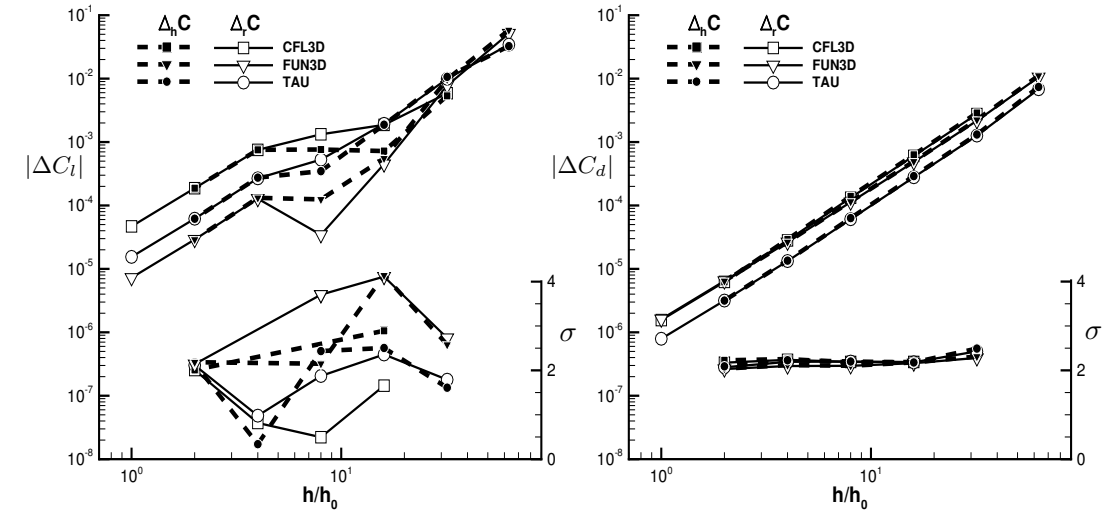

(a) $|\Delta C_l|$.

(b) $|\Delta C_d|$.

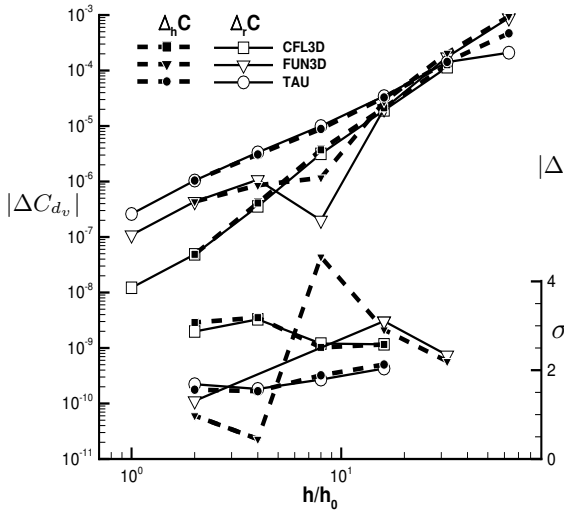

(c) $|\Delta C_{d_v}|$.

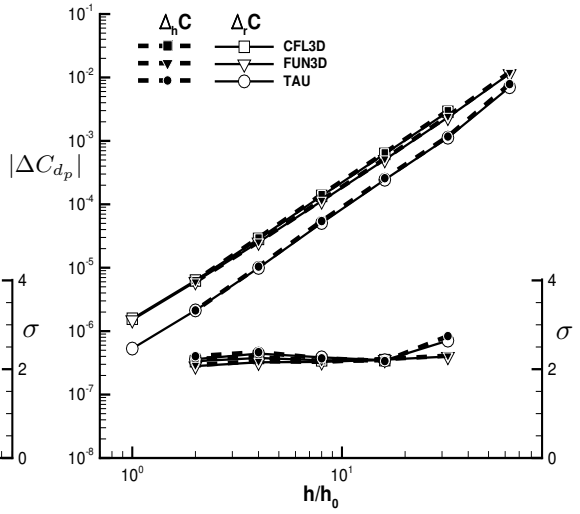

(d) $|\Delta C_{d_p}|$.

Figure 2. Error estimates and convergence rates of lift and drag coefficients. The upper set of curves shows the estimated errors and is associated with the left axis. The lower set shows the convergence rates and is associated with the right axis.

behavior, which is more pronounced in the Δ_r error estimate. Although all three CFD codes are converging on the finest grids, the convergence rates on grid-1 are influenced by the transition region, and none of the codes are showing a definitive trend of second-order convergence. On grid-1, CFL3D is converging at a rate of $\approx$3.0 and FUN3D is converging at a rate of $\approx$1.0. The TAU code is converging at a rate of 1.7 and is closest to its design order.

Contributions to drag from the pressure and viscous terms are similar in magnitude ($\approx$0.006). However, the estimated error of the viscous terms, ΔC_{d_v}, is lower than that of the pressure contribution by a factor ranging from approximately two for the TAU code, to one to two orders of magnitude for CFL3D and FUN3D. Consequently, the pressure contribution dominates the error estimate and convergence rate computations of the total drag, C_d. In the remainder of this work, plots of C_d are omitted whenever they are similar to C_{d_p}.

While the above figures do indicate that all properties are converging for all three CFD codes, they do not indicate whether the codes are converging to the same set of values. Figure 3 presents the difference between pairs of codes, denoted by Δ_c, as a function of mesh size. The viscous component of drag, C_{d_v}, is the only component for which all three codes are converging to the same value on the finest grid. The FUN3D and TAU codes are converging to the same C_{d_p} (C_d is not shown but is similar to C_{d_p}). Although the $\Delta_c C_{d_p}$ between FUN3D and CFL3D is small, the values have crossed and have begun to diverge on the three finer grids, and the divergence has stalled at $\approx 2.5 \cdot 10^{-6}$ finest grid. The largest difference between the codes occurs in the lift coefficient. The convergence rates have dropped noticeably on the finest grid suggesting that convergence may stall on yet finer grids. The error estimates $\Delta_r C_l$, are considerably smaller than $\Delta_c C_l$ and are on a convergent trend. Thus, the slowing of the convergence cannot be attributed to an interaction of the error estimates.

Table 1 gives the Richardson extrapolation for the four coefficients for each of the

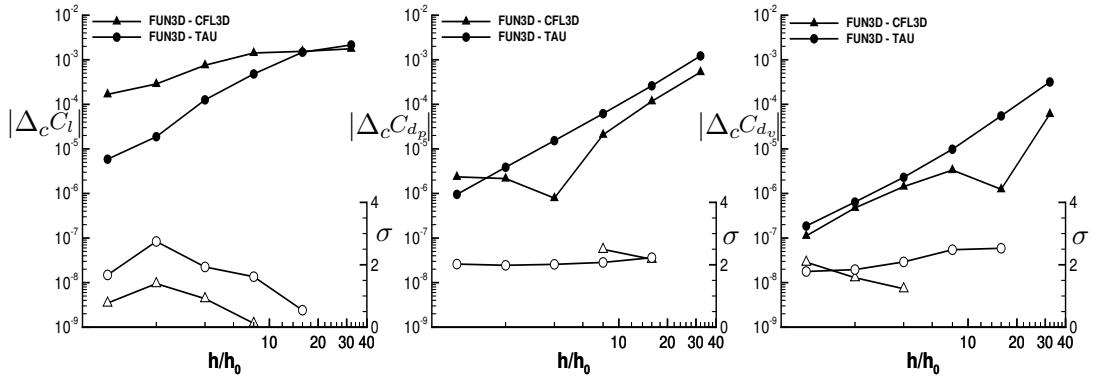

(a) Difference in C_l (b) Difference in C_{d_p} (c) Difference in C_{d_v}

Figure 3. Code to code comparisons of lift and drag coefficients. Solid symbol denotes $|\Delta_c C|$ and is associated with the left axis. Open symbol denotes the convergence rate, σ, and is associated with the right axis.

Table 1. Richardson extrapolation between two finest grids and the difference in the Richardson extrapolation between codes.

	C_l	C_d	C_{d_p}	C_{d_v}
CFL3D	1.09090048	0.012269991	0.006064194	0.006205797
FUN3D	1.09102833	0.012272406	0.006066618	0.006205788
TAU	1.09104242	0.012272462	0.006066638	0.006205823
|CFL3D - FUN3D |	$1.3 \cdot 10^{-4}$	$2.4 \cdot 10^{-6}$	$2.4 \cdot 10^{-6}$	$1 \cdot 10^{-8}$
|CFL3D - TAU |	$1.4 \cdot 10^{-4}$	$2.5 \cdot 10^{-6}$	$2.4 \cdot 10^{-6}$	$3 \cdot 10^{-8}$
|FUN3D - TAU|	$1.4 \cdot 10^{-5}$	$6 \cdot 10^{-8}$	$2 \cdot 10^{-8}$	$3 \cdot 10^{-8}$

three CFD codes. Also shown are the differences in the Richardson extrapolations between the codes, $\Delta_c U_r$. The difference in $C_{d_v,r}$ between any of the three codes is an order of magnitude smaller than the difference in the quantities themselves (Δ_h or Δ_h). The same is true for the differences between FUN3D and TAU codes for $C_{d,r}$ and $C_{d_p,r}$. The differences in $C_{d,r}$ and $C_{d_p,r}$ between CFL3D and either other code is similar to the difference in the property itself. For the Richardson extrapolation of the lift coefficient, $C_{l,r}$, the difference between codes is similar to or greater than the differences between C_l.

The Richardson extrapolation is most often thought of as an estimate of the limiting value of a quantity as the mesh size goes to zero. However, the Richardson extrapolation of a property can be computed between any two grids, and it provides a $(p+1)$-order approximation to that property. In the asymptotic regime, an estimate of the error in the Richardson extrapolation of a property, $\Delta_h U_r$, should be lower than the estimated error of the property itself, $\Delta_h U$ or $\Delta_r U$, and it should be converging at a higher rate (by one) than the property itself. This general rule is demonstrated in Appendix Section A.2 for monotone and oscillatory high-order models of the error. In practice, however, $\Delta_h U_r$ is a highly sensitive metric depending on Δ_h^2, and obtaining useful results is often difficult. Figures 4 and 5 present analogs to figures 2 and 3 in which some of the data has been replaced by its Richardson extrapolation.

Figure 4 is the analog to figure 2 in which $\Delta_h U$ has been replaced by $\Delta_h U_r$ (U denotes any of the force coefficients). The error estimate for the Richardson extrapolation of C_{d_p} is lower than the error estimate of C_{d_p} for all codes and for all grids (C_d is similar). As is typically the case in practice, the error estimate of the Richardson extrapolations is less smooth than that of the property itself, making calculations of convergence rates unreliable. However, the estimated error in the Richardson extrapolation of C_{d_p} essentially parallels that of the property, and therefore, the convergence rate is clearly not consistently higher than that computed directly from C_{d_p}. The estimated error of the Richardson extrapolation of the lift coefficient is generally lower than $\Delta_r C_l$ for the CFL3D and TAU codes, while the opposite is true of the FUN3D results. The convergence is not smooth, and valid convergence rates cannot be computed. Results for C_{d_v} are similar in character to those of C_l. Although the estimated error of the Richardson extrapolation of each

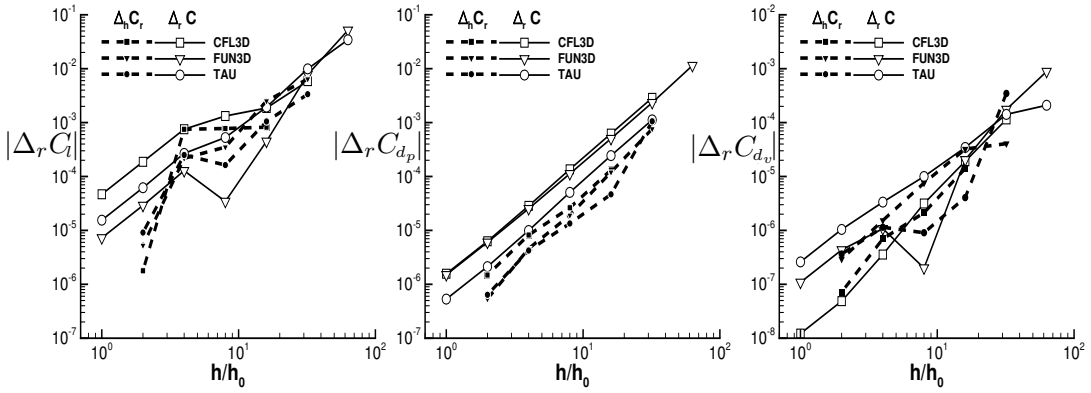

(a) Error estimates for C_l. (b) Error estimates for C_{d_p}. (c) Error estimates for C_{d_v}.

Figure 4. Error estimates of the Richardson extrapolation, $|\Delta_h C_r|$ of lift and drag coefficients compared to a direct estimate of error, .

coefficient is generally lower than that of the property itself, a $p+1$ convergence rate is not observed in any case. Formally, this would suggest that none of the results are within the asymptotic regime; however, it is more likely attributable to the ill-conditioned nature of this error estimate.

Code-to-code comparisons between the Richardson extrapolation of each force coefficient are presented in figure 5. This metric is smoother as it involves only a single Δ_h, and convergence rates can be reliably computed in most cases. Properties that previously exhibited an oscillatory convergence pattern in the metric $\Delta_c U$, converge monotonically in the $\Delta_c U_r$ metric, and vise versa. Generally, these results reinforce conclusions drawn from figure 3. In particular, Δ_c properties whose convergence had stalled, such as $\Delta_c C_{d_p}$ between FUN3D and CFL3D, are still stalled and at similar levels. Properties whose convergence was slowing, such as $\Delta_c C_l$, have now stalled. Some properties that were previously converging steadily, such as $\Delta_c C_{d_p}$ between FUN3D and Tau, are now showing signs of slowing convergence.

The notion of the Richardson extrapolation can be extended to higher order by fitting a higher degree polynomial form of the error model through data from more grids. Using a truncated and normalized form of equation 2 as a high-order error model

$$\epsilon(h) \equiv U(h) - U_e \approx \sum_{k=0}^{N-2} \alpha_k (h/h_0)^{p+k} \tag{4}$$

the parameters U_e and α_k can be determined by fitting equation 4 to data from a sequence of N grids. To denote that the results are obtained from a data fit to a particular set of grids, U_e is replaced by $U_{r_N,n}$ in which N denotes the number of grids included in the set, and n identifies the finest grid of the set. Thus, the fit is defined by

$$U_i = U_{r_N,n} + \sum_{k=0}^{N-2} \alpha_k (h_i/h_n)^{p+k} \tag{5}$$

for i in the interval $[n, n+N-1]$. As in the earlier results using the standard

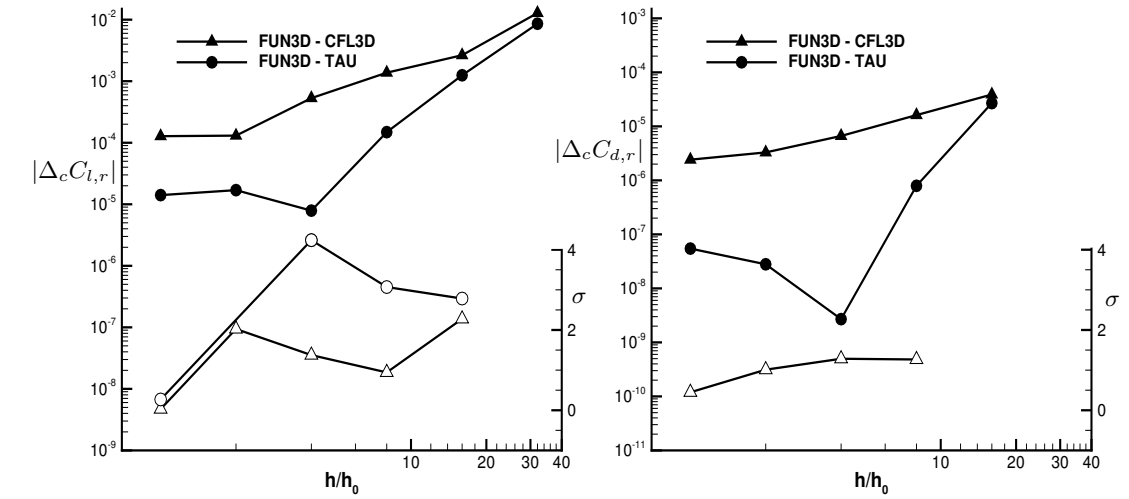

(a) $|\Delta_c C_{l,r}|$ and σ.

(b) $|\Delta_c C_{d,r}|$ and σ.

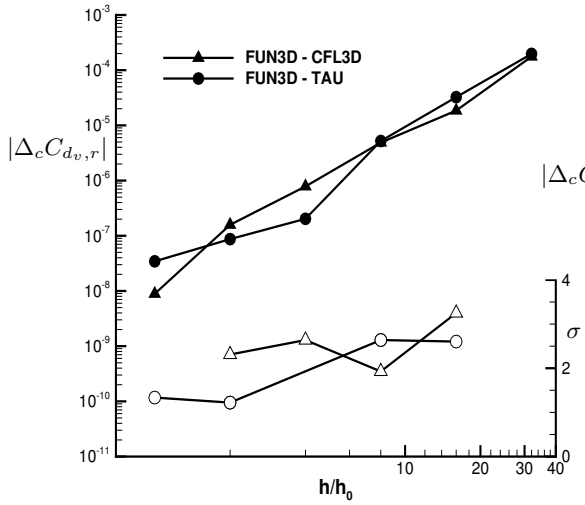

(c) $|\Delta_c C_{d_v,r}|$ and σ.

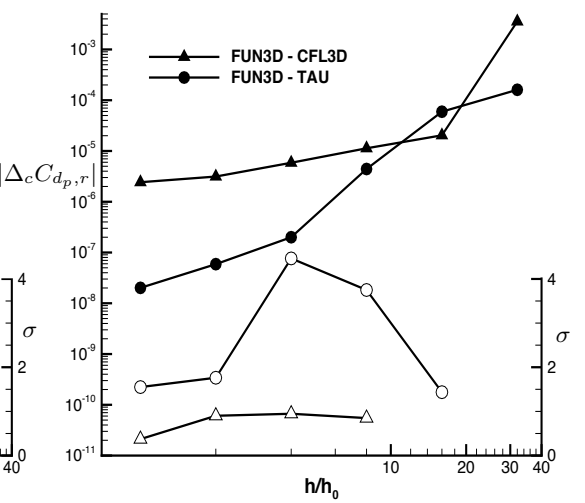

(d) $|\Delta_c C_{d_p,r}|$ and σ.

Figure 5. Code to code comparisons of the Richardson extrapolations of lift and drag coefficients. Solid symbol denotes $|\Delta_c C|$ and is associated with the left axis. Open symbol denotes the convergence rate, σ, and is associated with the right axis.

Richardson extrapolation, the design order of $p = 2$ is used in evaluating the data fit. Some additional details concerning this approach are discussed in the Appendix Section A.3. Note that $U_{r_2,n}$ is the standard Richardson extrapolation on grid-n. Also, to unify the notation, let $U_{r_1,n} \equiv U_i$. Figure 6 presents the convergence of the higher-order extrapolated solution in which the order of the fit is increased as the grid is refined. The plot shows the difference between the highest order extrapolation supported by a given grid and all coarser grids, and the next lower order extrapolation:

$$\Delta_N U_{r_N,n} \equiv U_{r_N,n} - U_{r_{N-1},n}. \tag{6}$$

This difference provides an indication of the accuracy of the high-order extrapolation. The high-order extrapolation converges faster than either the solution, or the Richardson extrapolation of the solution, and its convergence is smoother than the convergence of the Richardson extrapolation. The change in the high-order extrapolation on the finest grid is one to two orders lower than any error estimate of the solution given by Δ_h or Δ_r. Recall that, as was shown in figure 4, it is difficult to reliably estimate the error in the standard Richardson extrapolation.

Table 2 gives the high-order Richardson extrapolation, $U_{r_N,0}$, predicted using the highest-order extrapolation supported by the available grids ($N = 7$ for FUN3D and TAU results, $N = 6$ for CFL3D). The differences between the high-order Richardson extrapolations and the low-order Richardson extrapolations, shown in Table 1, are one to two orders of magnitude smaller than the code-to-code comparisons, except for those cases in which the code-to-code differences are less than 10^{-7}. Therefore, the code-to-code comparisons of the high-order Richardson extrapolations are similar to those shown in Table 1 for the standard low-order Richardson extrapolation in all cases (and are not shown here).

Another benefit of the high-order extrapolation is that it can provide a quantitative measure as to whether a set of grids has entered the asymptotic regime.

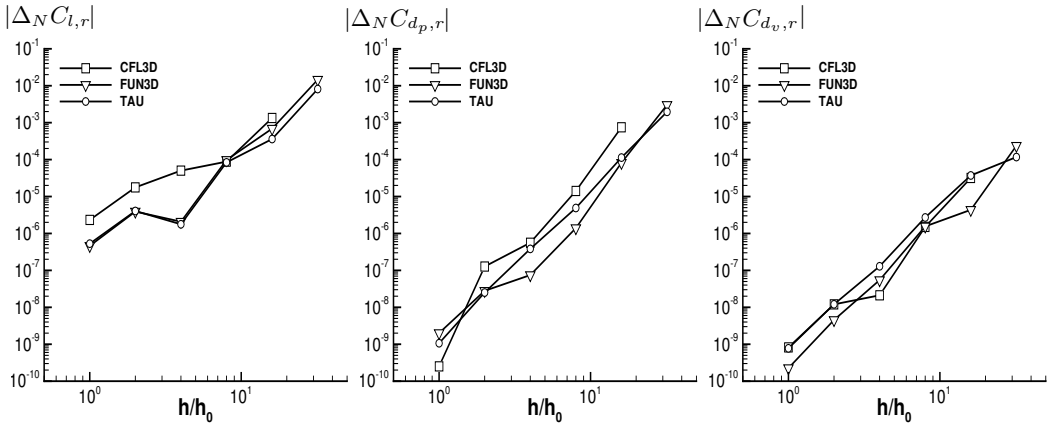

(a) $|\Delta_N C_{l,r_N,n}|$. (b) $|\Delta_N C_{d_p,r_N,n}|$. (c) $|\Delta_N C_{d_v,r_N,n}|$.

Figure 6. Convergence of high-order extrapolations, $|\Delta_N C_{r_N,n}|$, of lift and drag coefficients.

Table 2. Limit value from high-order Richardson extrapolation using all grids.

	C_l	C_d	C_{d_p}	C_{d_v}
CFL3D	1.0908884694	0.01227017647	0.006064383873	0.006205792595
FUN3D	1.0910231651	0.01227241020	0.006066662283	0.006205747916
TAU	1.0910359177	0.01227247257	0.006066708703	0.006205763868

Equation 5 can be recast as

$$U_j = U_{r_N,n} + \alpha_0 (h/h_0)^p \left[1 + \sum_{k=1}^{N-2} S_k (h/\hat{h}_k)^k \right], \tag{7}$$

in which $S_k = \text{sign}(\alpha_0 \alpha_k)$ and $\hat{h}_k \equiv h_0 |\alpha_0/\alpha_k|^{(1/k)}$. In this form, $\hat{h}_k$ is the grid size at which the magnitude of the k-th term is equal to that of the leading error term (the 0-th term). The smallest value of $\hat{h}_k$ can serve to mark the upper threshold of the asymptotic regime.

Table 3 gives the minimum value of $\hat{h}_k/h_0$ and identifies the term in which it occurs, k. For the current data sets in which the grid size doubles with each refinement, the grid ratios, h_k/h_0, are $\{1, 2, 4, 8, \ldots\}$ for $\{\text{grid-0}, \text{grid-1}, \text{grid-2}, \text{grid-3}, \ldots\}$. The threshold for C_{d_p} is just below grid-3 for CFL3D and TAU codes (e.g., $\hat{h}_k/h_0 = 7.4$ and 7.9 are just below $h_3/h_0 = 8$), and just below grid-4 for the FUN3D code. The threshold for C_{d_v} is lower for all three codes and is especially so for CFL3D and FUN3D. The threshold for C_l is less than one for all three codes suggesting that none of the grids are within the asymptotic regime for the lift coefficient. For C_l and C_{d_p}, the thresholds predicted by the high-order Richardson extrapolation are lower than might be inferred from a visual inspection of figures 2(a) and (d). It is interesting to note that the value of k associated with the smallest $\hat{h}_k$ is *not* always $p+1$ (as intuition might dictate), but that occasionally a higher order term indicates the onset of the asymptotic regime.

Table 3. Threshold of asymptotic regime for each force coefficient, and the term in which it occurred: $\hat{h}_k/h_0$, k.

	C_l	C_d	C_{d_p}	C_{d_v}
CFL3D	0.9, 1	7.4, 1	7.4, 1	2.2, 2
FUN3D	0.5, 1	13.6, 2	14.1, 3	4.9, 1
TAU	0.07, 1	10.4, 2	7.9, 1	6.1, 1

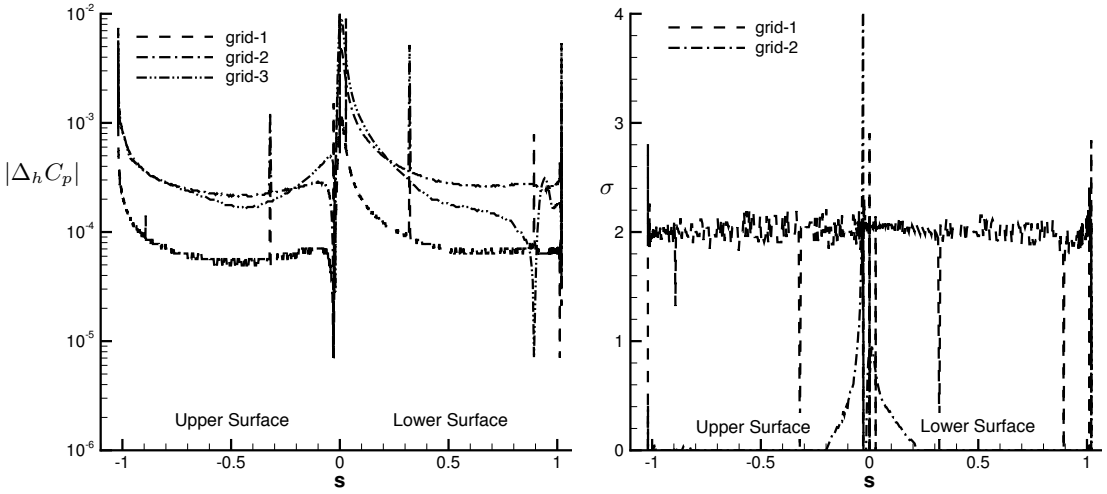

(a) $|\Delta_h C_p|$ for CFL3D.

(b) σ for CFL3D.

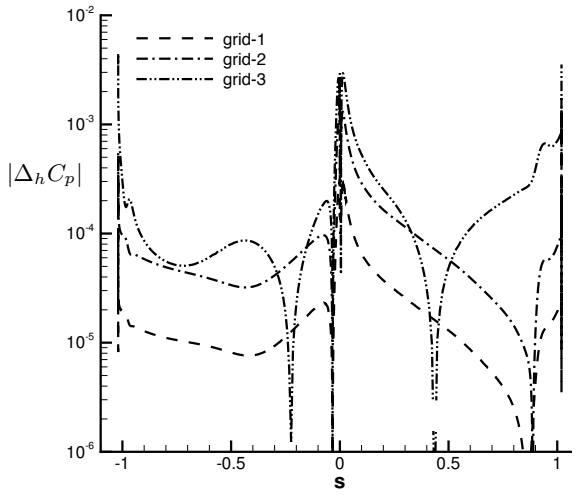

(c) $|\Delta_h C_p|$ for FUN3D.

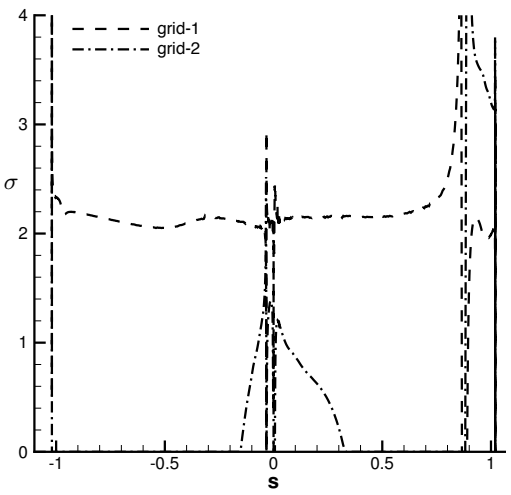

(d) σ for FUN3D.

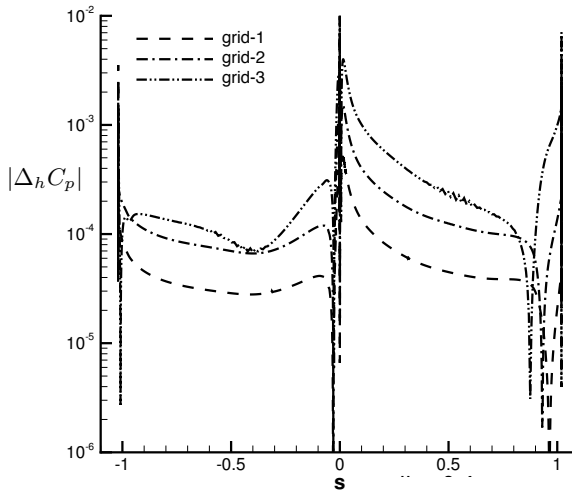

(e) $|\Delta_h C_p|$ for TAU.

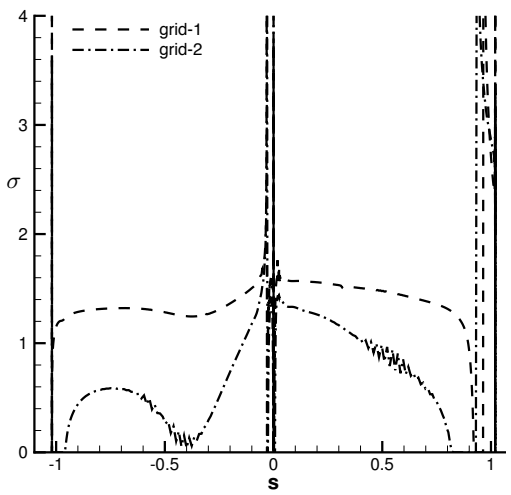

(f) σ for TAU.

Figure 7. Pointwise $|\Delta_h C_p|$ on airfoil surface and associated convergence rates, σ.

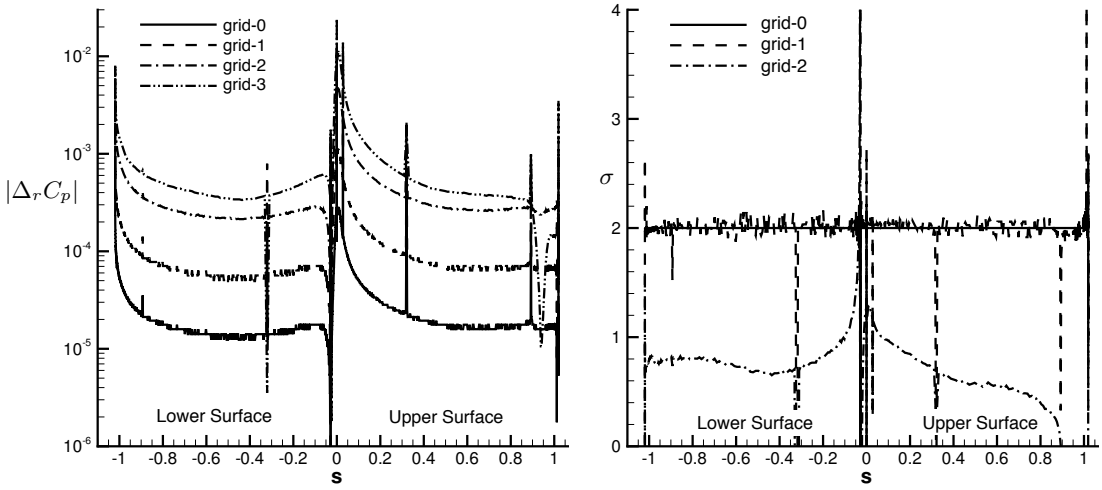

(a) $|\Delta_r C_p|$ for CFL3D.

(b) σ for CFL3D.

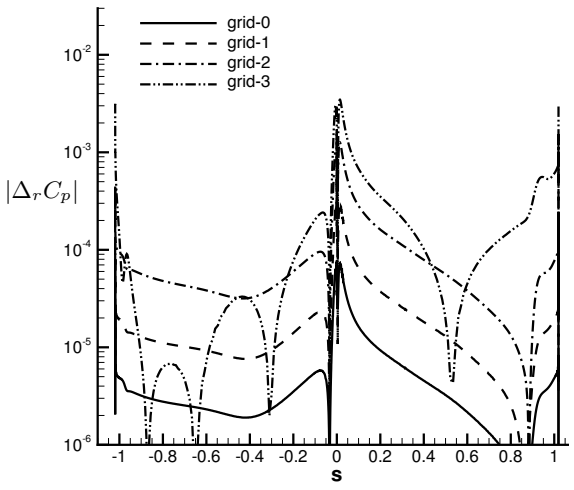

(c) $|\Delta_r C_p|$ for FUN3D.

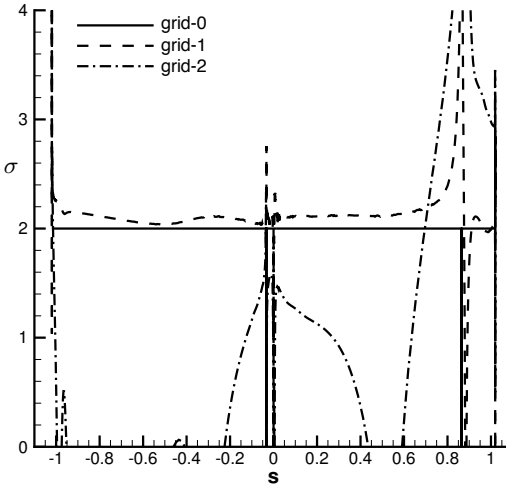

(d) σ for FUN3D.

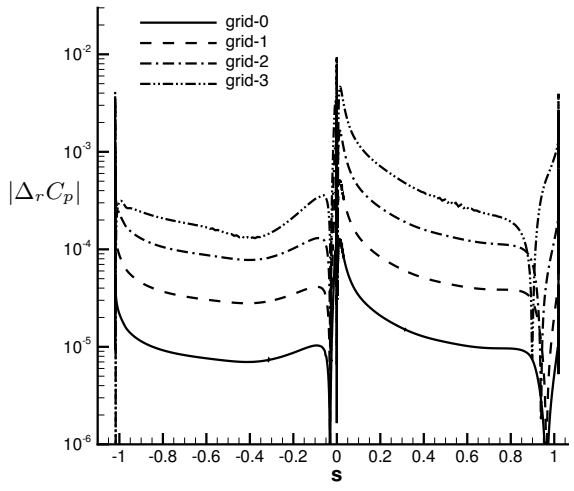

(e) $|\Delta_r C_p|$ for TAU.

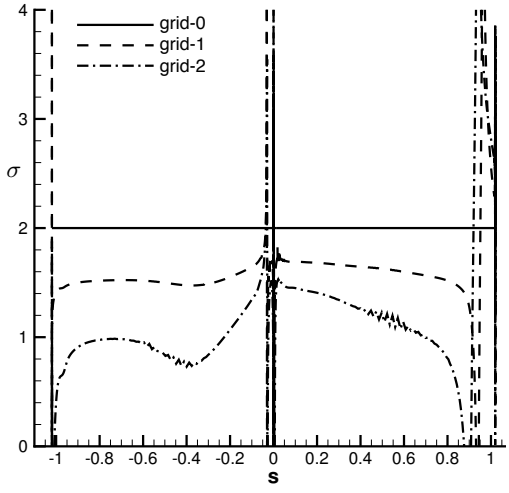

(f) σ for TAU.

Figure 8. Pointwise $|\Delta_r C_p|$ on airfoil surface and associated convergence rates, σ.

exactly second order. Here the convergence rates are presented only to illustrate this point. A major distinction between figures 7 and 8 is in the behavior of the coarsest grids. Except for small isolated regions, $\Delta_r C_p$ for the CFL3D and TAU codes are converging monotonically. Only the lower surface of FUN3D shows significant regions of nonmonotone convergence. Another distinction between figures 7 and 8, that is especially noticeable for the TAU results, is that the convergence rates on grid-1 are closer to the design order.

The convergence rates for the second finest grid in figures 7 and 8 should agree closely if the solutions are well within the asymptotic regime. However, because $\Delta_h C_{p,1} \equiv \Delta_r C_{p,1}$ and $\Delta_r C_{p,0} \equiv \Delta_r C_{p,1}/4$, differences in the convergence rate on grid-1, $\sigma(\Delta_h C_{p,1})$ and $\sigma(\Delta_r C_{p,1})$, are in fact completely determined by the error level on grid-2, $\Delta_h C_{p,2}$ and $\Delta_r C_{p,2}$.

Figures 9 and 10 present the convergence of C_{f_x} using Δ_h and Δ_r respectively. Because of missing data in the CFL3D data files, only results for FUN3D and TAU are presented. The estimated errors of FUN3D are generally lower on the lower surface than on the upper surface. The opposite is true for the TAU code. As with C_p, the estimated error of C_{f_x} has peaks near the leading and trailing edges. These peaks are larger for the TAU code than for FUN3D. The distribution and character of the estimated error on the upper surface is similar between the two codes. However, the error of the TAU code on the lower surface is much more evenly distributed. Convergence is generally monotone on both surfaces for both codes, however, the error drop between finer grids is less than that observed on the coarser grids in some regions. This is particularly evident on the lower surface of data produced by the TAU code in figure 9. Comparing figures 9 and 10, the results are very similar in character; however, many of the unusual attributes just described are less pronounced when using the Δ_r error measure. For example, in some regions, the error drop between the finer grids is still less than that between the coarse grid but not to the degree observed in figure 9. Accordingly, the convergence rates computed from Δ_r are closer to the design order, especially on the lower surface for data produced by the TAU code.

Finally, figure 11 presents pointwise code-to-code comparisons of C_p on the airfoil surface. The agreement between the codes is converging uniformly everywhere except in the immediate vicinity of the leading and trailing edges. The differences between FUN3D and TAU codes are about an order of magnitude lower than the differences between the FUN3D and CFL3D codes. The large drop in the differences between the FUN3D and TAU codes between the finest grids is somewhat misleading. A close examination of the differences reveals that the sign of the differences have changed, indicating that the solutions have crossed and will begin to diverge. This is confirmed by the differences in the Richardson extrapolations, which are significantly larger than the differences on the finest grids (shown as a dashed line with open circles). This is further confirmed by the high-order extrapolation through all four grids for which the differences are higher still (shown by the dotted line with open triangles). For the differences between FUN3D and CFL3D, both extrapolations are the same (to within the noise in the data) and are slightly lower than the differences between those two codes on the finest grids.

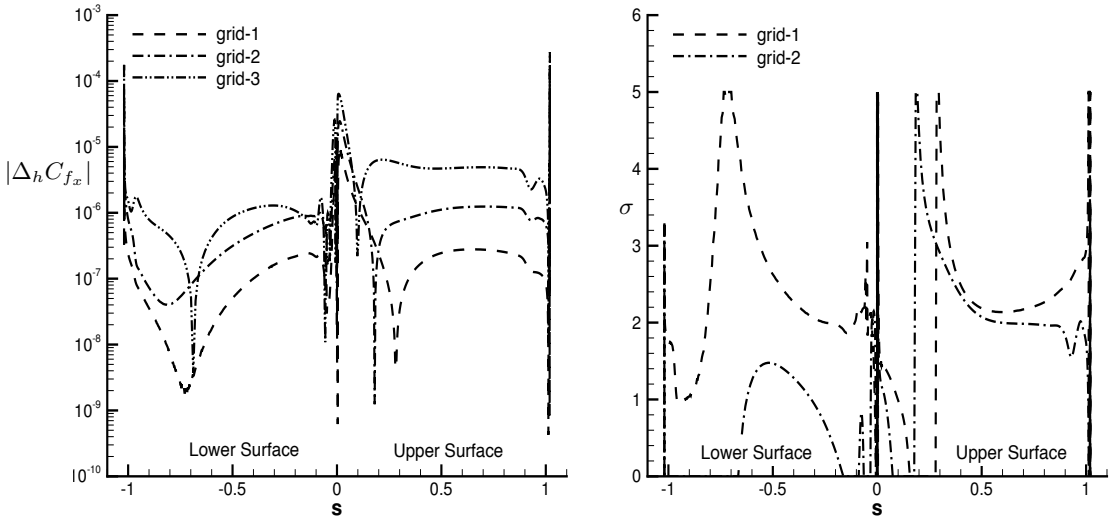

(a) $|\Delta_h C_{f_x}|$ for FUN3D.

(b) σ for FUN3D.

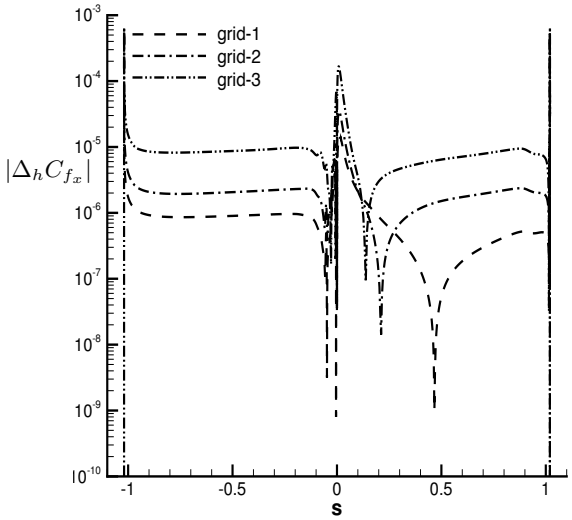

(c) $|\Delta_h C_{f_x}|$ for TAU.

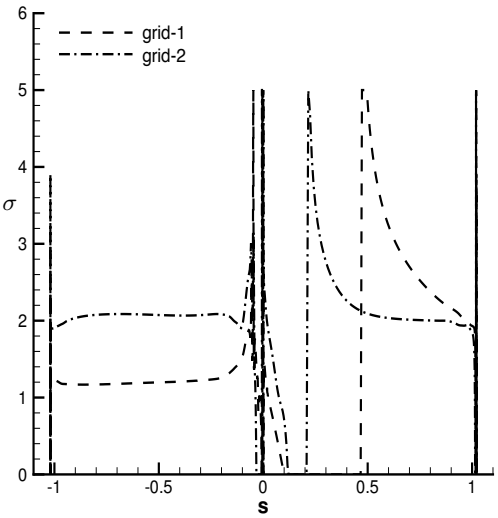

(d) σ for TAU.

Figure 9. Pointwise $|\Delta_h C_{f_x}|$ on airfoil surface and associated convergence rates, σ.

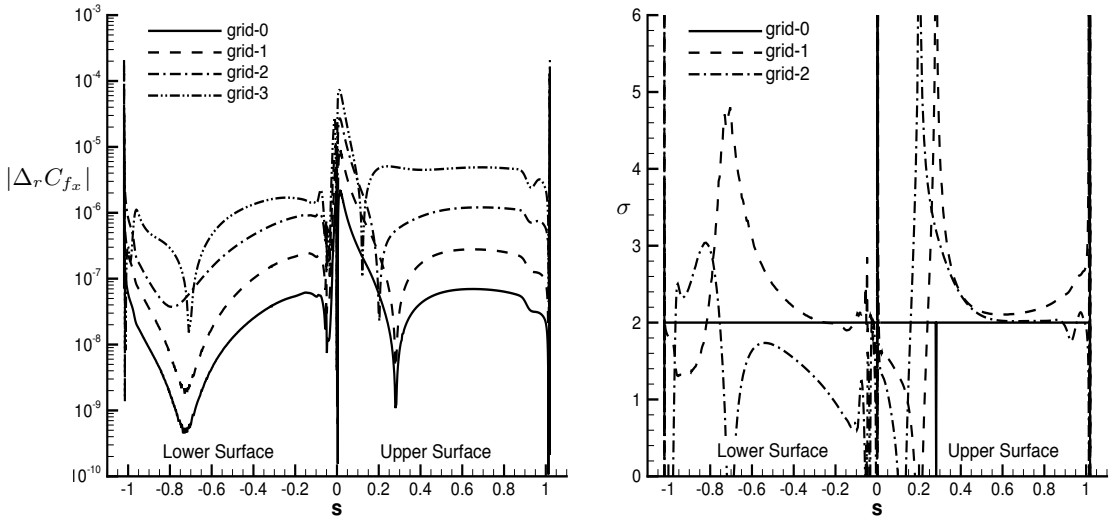

(a) $|\Delta_r C_{f_x}|$ for FUN3D.

(b) σ for FUN3D.

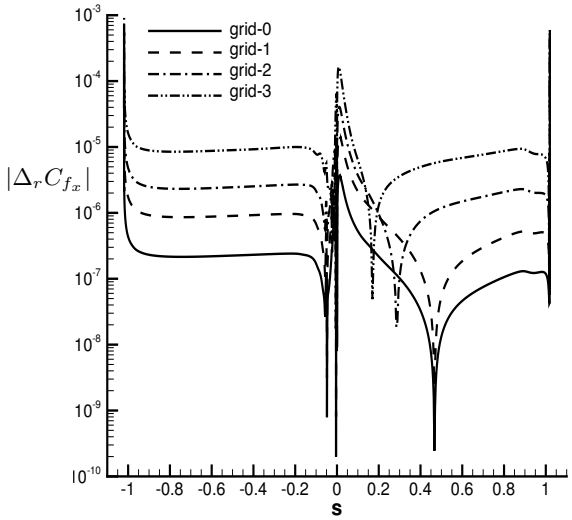

(c) $|\Delta_r C_{f_x}|$ for TAU.

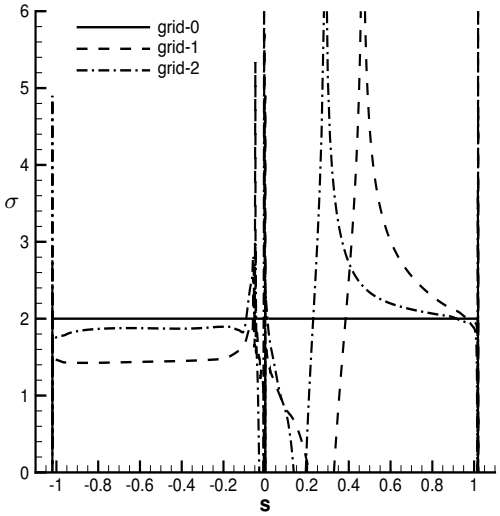

(d) σ for TAU.

Figure 10. Pointwise $|\Delta_r C_{f_x}|$ on airfoil surface and associated convergence rates, σ.

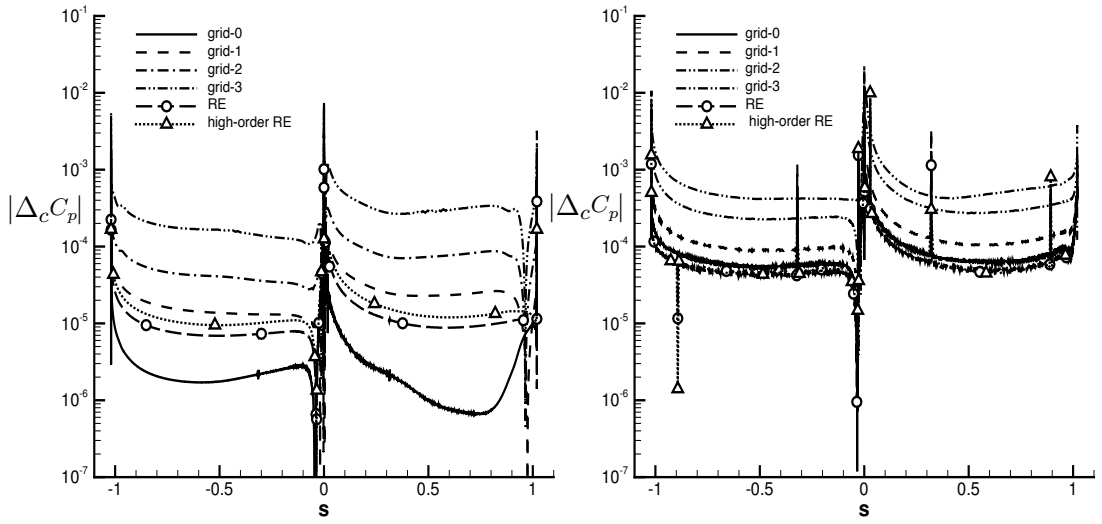

(a) Difference in C_p between FUN3D and TAU codes.

(b) Difference in C_p between FUN3D and CFL3D codes.

Figure 11. Pointwise code to code comparison of C_p on airfoil surface.

4 Data Diagnostics

The convergence analysis of the pointwise data can provide insight into the discretization and uncover irregularities that are not apparent by examination of the solution directly, but that may be reducing the accuracy and efficiency of the simulation. The plots of estimated error in figures 7 through 10 contain four types of irregularities. The first type of irregularity examined is indicated by the piecewise smooth downward spikes seen in the data for all codes at almost all grid levels. For example, such spikes occur in figure 7(c) near $s = -0.2$, 0.4 and 0.9. These downward spikes will occur in $\Delta_h U$ whenever solutions on adjacent grids intersect, and in $\Delta_r U$ whenever the solution intersects the Richardson extrapolation. Such spikes are common and normal, but they have consequences. The depth of the downward spike has no physical or numerical significance, but is merely a function of how close to a grid point the intersection occurs. However, the small values of estimated error corrupt the convergence rate computation on two grid levels, causing the computed order property to approach plus or minus infinity depending on whether the small value appears in the numerator or denominator of equation 3. For global or integrated quantities, such behavior is commonly associated with oscillatory convergence and is often an indicator that the solution is not in the asymptotic regime. However, this is not the case for pointwise error estimates as the solution intersections and associated downward spikes often appear on every grid. The downward spikes may shift during grid refinement by an amount that decreases with refinement. The shifts can be associated with phase errors in the solution, but more commonly result from different regions of the flow converging at different rates. An integrated quantity is strongly influenced by the shifting of a downward spike, resulting in oscillatory convergence of the integrated quantity even when the pointwise solution is converging

monotonically in regions away from the spike. The convergence rate computation is corrupted in a region in the neighborhood of the downward spike, and this region is larger if the downward spike is shifting as the grid is refined. In the asymptotic regime, the physical width of the corrupt region tends to remain a constant as the mesh is refined.

The second type of irregularity is indicated by the upward spikes near the leading and trailing edges. Both regions have complex physics and higher than average gradients that may challenge the numerics. However, the grids are highly refined in these region, and numerical experiments to assess the sensitivity of the trailing edge resolution have been performed (ref. 2). Figure 12a presents $\Delta_h C_p$ near the leading edge for data produced by the TAU code. The piecewise smooth downward spikes near $s = -0.03$ and 0.005 are of the type described previously and are not a concern. Figure 12b expands the scale further near $s = 0.0$, but also includes the stagnation point, which is at approximately $s = -0.00273$. The estimated errors are smooth near the stagnation point suggesting that this complex flow region causes no unusual difficulties. At $s = 0.0$, however, the geometry, the solution, and all boundary conditions are smooth and yet the error is not. Figure 13 presents $\Delta_h C_p$ near the leading edge for all three codes where it is clear that the problem is not isolated to the TAU code. Unlike the first type of irregularity, the region affected by the oscillations is limited to a few grid points near $s = 0$, so the physical region affected becomes smaller as the mesh is refined. The relative amplitude of the spike in the error of the CFL3D and TAU codes decays slower than that of surrounding points as the grid is refined. FUN3D has the smallest oscillations, and the irregularity at $s = 0$ takes on the character of a jump in error as the grid is refined (rather than a spike or oscillation).

Considering the smoothness of the geometry and the expected smoothness of the

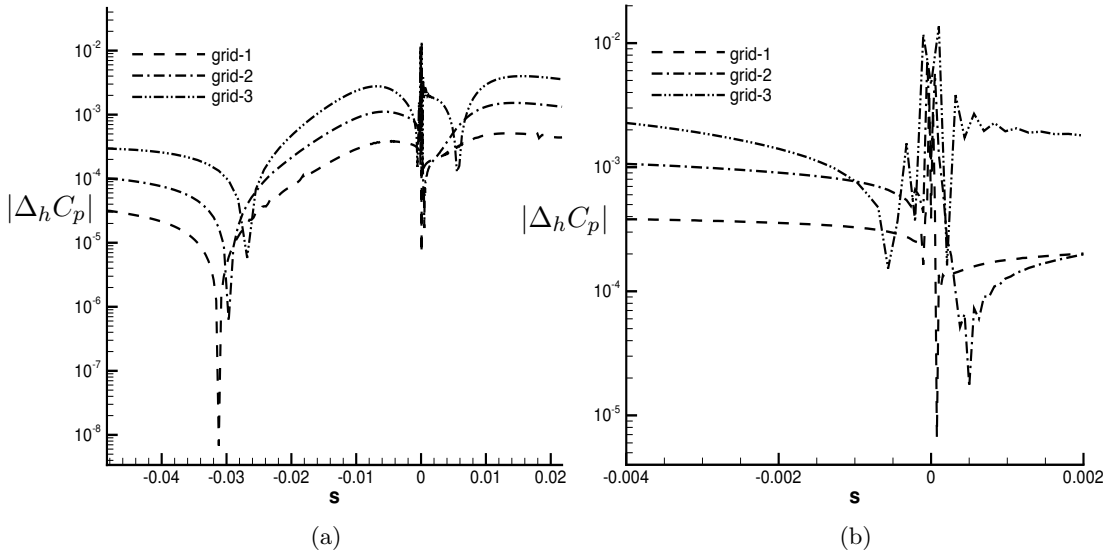

Figure 12. Pointwise convergence of $|\Delta_h C_p|$ near leading edge for TAU code.

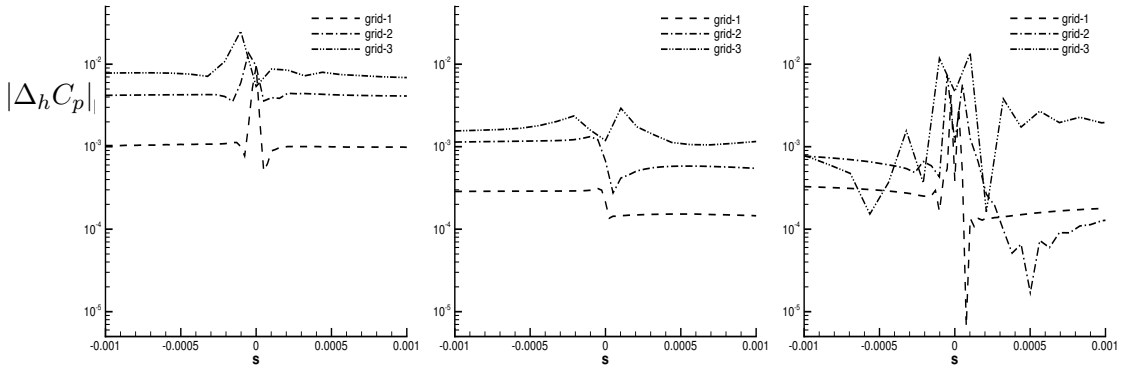

(a) $|\Delta_h C_p|$ for CFL3D. (b) $|\Delta_h C_p|$ for FUN3D. (c) $|\Delta_h C_p|$ for TAU.

Figure 13. Pointwise convergence of $|\Delta_h C_p|$ near the leading edge.

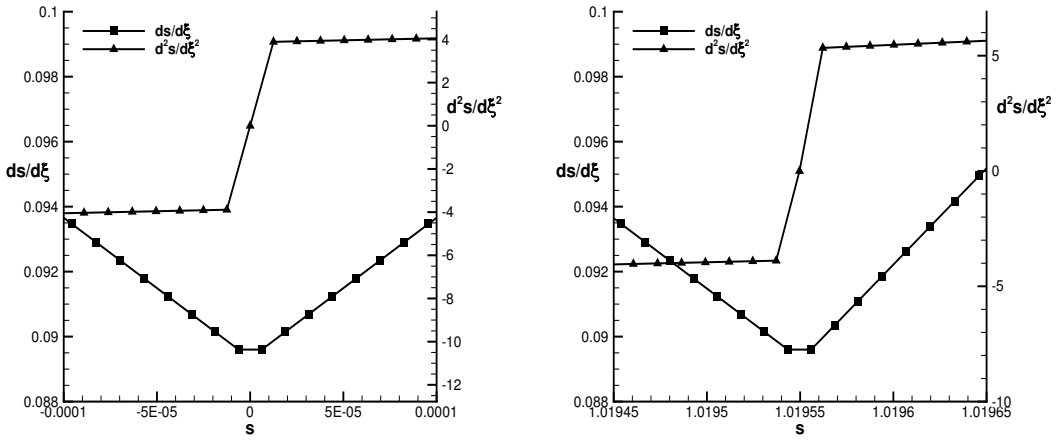

(a) Near leading edge. (b) Near trailing edge.

Figure 14. Grid spacing and the derivative of the grid spacing near leading edge.

flow at $s = 0$, a probable cause for the oscillations is a lack of smoothness in the grid. When viewed directly, the grid near the leading edge appears essentially uniform in the direction around the airfoil. However, a close examination of the derivatives of the grid, shown in figure 14, indicates that the normalized grid spacing $ds/d\xi$ is continuous but not differentiable at $s = 0$ (note: $\xi = i/I_{\max}$). A similar jump in the derivative of the mesh spacing $d^2s/d\xi^2$ occurs at both the leading and trailing edges of the airfoil. An examination of other aspects of the grid reveals that the wall-normal stretching is slightly nonuniform near the leading and trailing edges; however, its variation is slight and appears continuous. CFL3D is a structured grid code that relies on a smooth curvilinear grid transformation, thus it is not surprising that a nonsmooth grid might produce some error. It is generally thought that the unstructured grid codes should be less sensitive to grid smoothness, as they are designed for unstructured grids that are inherently nonsmooth. However, the errors produced by the two unstructured grid codes are substantial, and they have quite

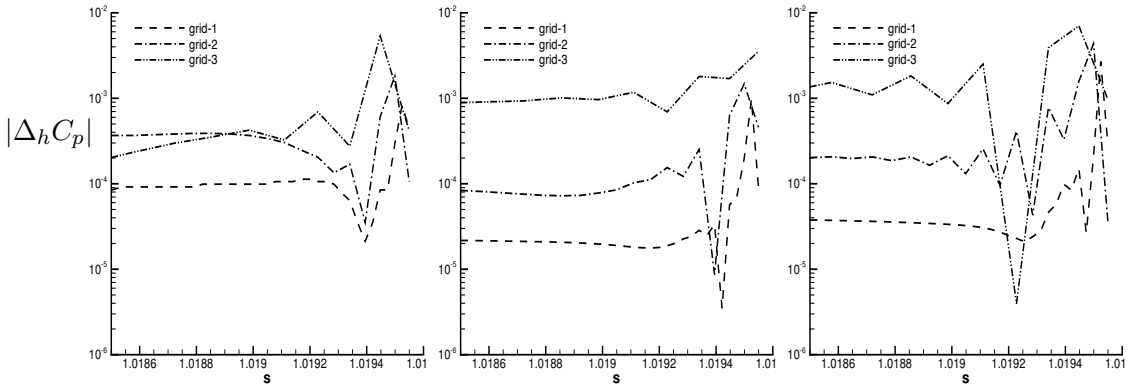

(a) $|\Delta_h C_p|$ for CFL3D. (b) $|\Delta_h C_p|$ for FUN3D. (c) $|\Delta_h C_p|$ for TAU.

Figure 15. Pointwise $|\Delta_h C_p|$ near the trailing edge upper surface.

different characteristics from one another.

As noted above, the grid near the trailing edge also has discontinuous metrics. Error spikes and oscillations near the trailing edge, shown in figure 15, are similar in character to those at the leading edge. That is, the oscillations in the error are limited to a few points near the trailing edge, and the amplitude of the oscillations converges much more slowly than points just upstream of the trailing edge. While the flow near a sharp trailing edge is known to have singular attributes (refs. 2, 14), the affected region scales with Reynolds number as $Re^{-3/4}$ (refs. 15, 16). For the current case with a Re=$6 \cdot 10^6$, the singular behavior is expected to be contained within a radius of $\approx 8 \cdot 10^{-6}$, which is on the order of the streamwise mesh spacing of the finest grid. Thus, the singular behavior is wholly unresolved by the sequence of grids in this study, and the discontinuous grid metric may be contributing to the trailing edge oscillations.

The third type of irregularity is indicated by the highly isolated spikes seen in the CFL3D data in figures 7 and 8. These spikes occur at four positions on both the upper and lower surfaces: $s \simeq \pm 0.028$, ± 0.32, ± 0.89 and $\pm\, 1.012$. A close examination of the data at $s \simeq 0.32$, shown in figure 16, reveals that the nonsmoothness is limited to a single grid point on the two finest grids. The two coarser grids are unaffected. At two of the stations, $s \simeq \pm 0.028$ and ± 1.012, only the finest grid is affected. In addition, C_{f_x} data for these points are missing from the file `cfl3d_cf_sa_nopv.dat`. After some investigation (ref. 17), it has been determined that the finer grid simulations using CFL3D employed that method's multiple-block capability, and that the four streamwise stations given above coincide with the block boundaries. The discrepancies have been identified as being associated with post processing of the CFL3D data to interpolate the data from the cell-centered locations to the node locations.

Finally, the fourth irregularity is the noisy character of the CFL3D data mentioned earlier. A close examination of the data in a region where C_p is nearly constant is shown in figure 17. On the finest grid, C_p has an unexpected piecewise linear character. This occurs in spite of the fact that the data in the file contains

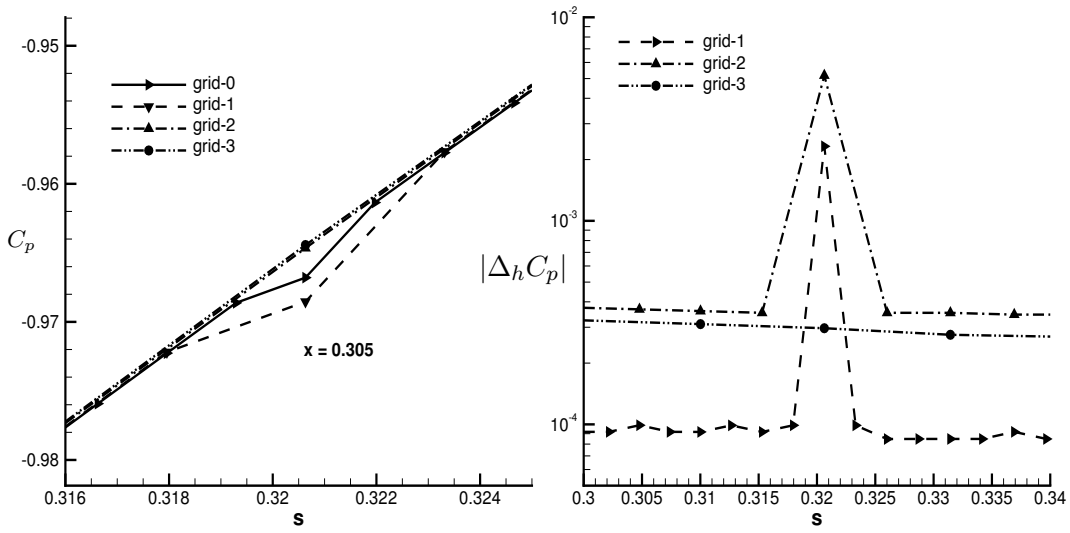

(a) C_p. (b) $|\Delta_h C_p|$.

Figure 16. C_p and $|\Delta_h C_p|$ near error spike in CFL3D data.

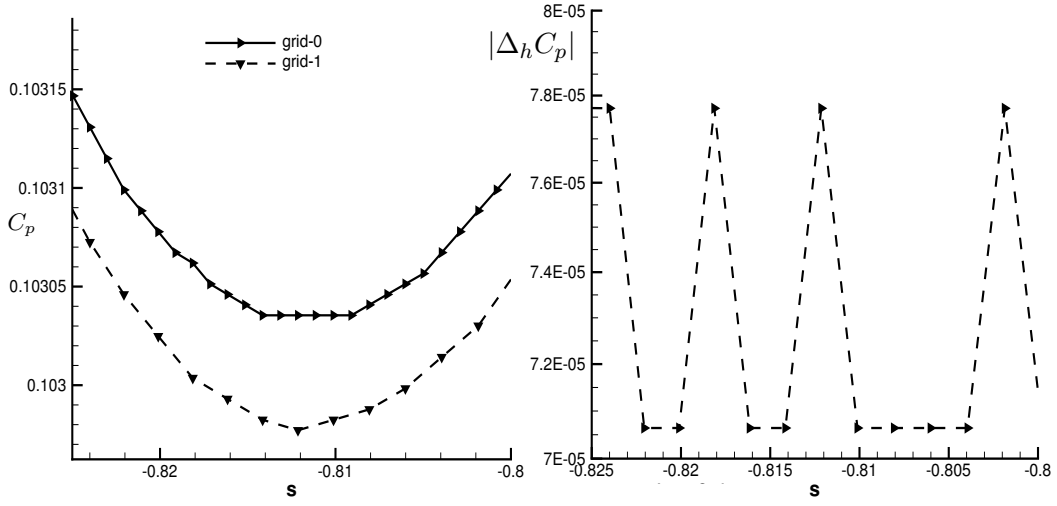

(a) C_p. (b) $|\Delta_h C_p|$ between grid-0 and grid-1.

Figure 17. C_p and $\Delta_h C_p$ of CFL3D data in a region where C_p is nearly constant.

10 significant figures. Although smoother in appearances, the second finest grid also exhibits a slight nonsmoothness; however, it is less noticeable because there are no regions that are sufficiently constant. This abnormality is consistent with a truncation in precision to $\approx 5 \cdot 10^{-6}$, which corresponds to the precision of single precision data. It is suspected that single precision operations were used at some point during the post processing to interpolate data to the nodes.

None of the irregularities just discussed are readily apparent through a direct examination of the solution. The pointwise convergence analysis has not only made them apparent, but has also provided clues to their cause. The first type of irregularity, the downward spike caused by intersecting solutions, is common and is of little concern. However, it is important to recognize that order property estimates will be invalid in the neighborhood of this type of irregularity. The remaining three types of irregularities (the oscillations near leading and trailing edges exhibited by all three codes, the single point spikes at particular locations, and the low level noise in the CFL3D data) were indicative of a potential problem with grid smoothness, or with the extraction and post processing of the data. The second and third type of irregularities were isolated to a finite number of grid points. The fourth type of irregularity was global but its amplitude was about on order of magnitude smaller than the measured errors on the finest grid. Consequently, it is not expected that any of the irregularities has a significant impact on the flow solution, or that correcting them would alter any conclusions drawn in prior publications.

5 Summary

Data from the "Turbulence Modeling Resource" website are analyzed to determine the convergence behavior of three second-order CFD codes: CFL3D, FUN3D and TAU. The case considered for this analysis is the simulation of turbulent flow over an NACA–0012 airfoil using the Spalart-Allmaras turbulence model. The convergence of both integrated properties and pointwise data are examined. Several different methods for estimating errors and computing convergence rates are also compared. The coefficient of drag exhibits second-order convergence for all three codes, and convergence is monotone over a sequence of 7 grids. The convergence rates of other properties are less well behaved. Although the viscous and pressure components of drag are similar in magnitude ($\approx$0.006), the error in the pressure component is much larger and dominates the convergence properties. The errors in the viscous component of drag predicted by CFL3D and FUN3D are one to two orders lower than that due to pressure. The convergence rates of the viscous component on the three finest grids ranges from $\approx$3.0 for CFL3D to $\approx$1.0 for FUN3D. The error of the viscous component predicted by the TAU code is only a factor of two lower than that of the pressure component, and the convergence rate is $\approx$1.6.

Two methods for estimating the error, Δ_h and Δ_r, give similar results within the asymptotic regime. Neither method is particularly reliable for coarser grids, and disagreement between them serves primarily to confirm that the CFD methods are outside the asymptotic regime (for that particular data). The extent of the asymptotic regime is not a fixed property of a code and the flow case, but also

depends on the physical property under examination. While the total drag and the contribution due to pressure appear to be within the asymptotic regime for all grids, only the two or three finest grids appear to be within the asymptotic regime for the lift and the viscous component of drag. However, as it takes more than three grid levels to establish a trend, there is uncertainty whenever only the three finest grids appear to be within the asymptotic regime. A high-order extension to the Richardson extrapolation improves the accuracy of the mesh limit values, and provides a quantitative estimate of the threshold of the asymptotic regime. This approach indicates that the lift is not in the asymptotic regime on even the finest grid for any of the three CFD codes. For the viscous component of drag, CFL3D results are within the asymptotic regime on the two finest grids, whereas FUN3D and TAU results are within asymptotic regime on the three finest grids.

The three codes are converging to similar but not identical solutions. The largest differences between the codes are in the coefficient of lift for which the difference between CFL3D and FUN3D is greater than 10^{-4}. The best agreement occurs in the viscous component of drag in which all three codes are converging toward each other at second-order. The agreement between the two unstructured grid codes is good with all properties except lift converging toward common values at a rate of second-order.

Analysis of pointwise data on the four finest grids provides insight into the error distribution. For all three codes, the error in C_p is generally lower and more uniformly distributed on the lower surface of the airfoil than on the upper surface. FUN3D has the lowest error in C_p on the lower surface, but exhibited the least uniformity on the upper surface. The different error estimates give similar results for the three finest grids, but are noticeably different on the coarsest of the four grids indicating that the coarsest grid is outside of the asymptotic regime. All three codes exhibit spikes in the error of C_p at the leading and trailing edge.

Examination of C_{f_x} from the FUN3D and TAU codes indicates that the two error estimates give similar results on all four grids. The C_{f_x} of both codes exhibited spikes at the leading and trailing edges, but otherwise, the two codes have very different error distributions. For FUN3D, the estimated error on the upper surface is higher and more uniform than on the lower surface, while the opposite is true for the TAU results. Convergence rates are highly nonuniform, and rates on the finest grids are further from the design order than those on the coarser grids.

References

1. "Turbulence Modeling Resource Website," [online database], NASA Langley Research Center, VA, http://turbmodels/larc.nasa.gov [retrieved 6 Dec. 2017].

2. Diskin, B., Thomas, J. L., Rumsey, C. L., and Schwöppe, A., "Tetrahedral Unstructured Navier-Stokes Method for Turbulent Flows," *AIAA Jounal*, Vol. 36, No. 11, 1998, pp. 1975–1982.

3. Thomas, J. L., Krist, S., and Anderson, W., "Navier-Stokes Computations of Vortical Flows Over Low-Aspect-Ratio Wings," *AIAA Journal*, Vol. 28, No. 2, 1990, pp. 205–212.

4. "CFL3D Version 6 Website," [online], NASA Langley Research Center, VA, http://cfl3d/larc.nasa.gov [retrieved 11 June 2018].

5. Anderson, W. K. and Bonhaus, D. L., "An Implicit Upwind Algorithm for Computing Turbulent Flows on Unstructured Grids," *Computers and Fluids*, Vol. 23, No. 1, 1994, pp. 1–22.

6. Biedron, R. T., Carlson, J.-R., Derlaga, J. M., Gnoffo, P. A., Hammond, D. P., Jones, W. T., Kleb, B., Lee-Rausch, E. M., Nielsen, E. J., Park, M. A., Rumsey, C. L., Thomas, J. L., and Wood, W. A., "FUN3D Manual: 13.2," NASA/TM-2017-219661, August 2017.

7. Schwöppe, A. and Droll, N., "The DLR Flow Solver TAU – Status and Recent Algorithmic Developments," AIAA Paper 2014-0080, January 2014.

8. Richardson, L. F., "The Approximate Arithmetical Solution by Finite Differences of Physicsl Problems involving Differential Equations, with an Application to the Stresses in a Masonary Dam," *Philosophical Transitions of the Royal Society of London, Series A*, Vol. 210, 1911, pp. 307–357.

9. Warming, R. F. and Hyett, B. J., "The Modified Equation Approach to the Stability and Accuracy Analysis of Finite-Difference Methods," *Jounal of Computational Physics*, Vol. 16, No. 2, 1974, pp. 159–179.

10. Roache, P. J., *Verification and Validation in Computational Science and Engineering*, Hermosa publishers, 1998.

11. Richardson, L. F. and Gaunt, J. A., "The Deferred Approach to the Limit. Part I. Single Lattice, Part II. Interpeneting Lattices." *Philosophical Transitions of the Royal Society of London, Series A*, Vol. 226, 1927, pp. 229–361.

12. Celik, I. B., Ghia, U., Roache, P. J., Freitas, C. J., Coleman, H., and Raad, P. E., "Procedure for Estimation and Reporting of Uncertanty Due to Discretization in CFD Applications," *ASME Journal of Fluids Engineering*, Vol. 130, 2008, pp. 307–357.

13. Celik, I. B. and Karatekin, O., "Numerical Experiments on Application of Richardson Extrapolation with Nonuniform Grids," *ASME Journal of Fluids Engineering*, Vol. 119, 1997, pp. 584–590.

14. Golestein, S., "Concerning some solutions of the boundary layer equations in hydrodynamics," *Proceedings of the Cambridge Philosophical Society*, Vol. 26, 1930, pp. 1–30.

15. Stewartson, K., "On the Flow Near the Trailing Edge of a Flat Plate II," *Mathematika*, Vol. 16, 1969, pp. 106–121.

16. Messiert, A. F., "Boundary-layer Flow Near the Trailing Edge of a Flat Plate," *SIAM Journal on Applied Mathematics*, Vol. 18, 1970, pp. 241–257.

17. 2018, Rumsey, Christopher L, Private communications concerning CFL3D grids and post processing.

18. Salas, M. D. and Atkins, H. L., "On problems associated with grid convergence of functionals," *Computers & Fluids*, Vol. 38, No. 7, 2009, pp. 1445–1454.

Appendix A

Computation of Error Estimates and Convergence Rates

In the limit as the mesh size h goes to zero, the *numerical* error in the solution of a CFD simulation is expected to behave as

$$\epsilon(h) \equiv U(h) - U_e = \alpha h^p, \tag{A1}$$

in which the design order of convergence p is a property of the CFD discretization, and the coefficient α depends on both the solution and the discretization. If the exact solution is known, α and p can be determined by fitting the error model, equation A1, to data from any two grids:

$$\epsilon(h_i) \equiv U(h_i) - Ue = \alpha h_i^{\sigma}, \quad \text{for } i = 1, 2, \tag{A2}$$

in which p is replaced by σ to reflect that it is the result of a curve fit and not necessarily the order property of the CFD method. Dividing one equation into the other gives

$$\frac{\epsilon(h_2)}{\epsilon(h_1)} \equiv \frac{U(h_2) - Ue}{U(h_1) - Ue} = \left(\frac{h_2}{h_1}\right)^{\sigma}, \tag{A3}$$

and solving for σ gives

$$\sigma = \log\left(\frac{U(h_2) - Ue}{U(h_1) - Ue}\right) / \log\left(\frac{h_2}{h_1}\right). \tag{A4}$$

The coefficient α can be determined from equation A2 using data from either grid-1 or grid-2.

If the exact solution is not known, as is usually the case, a surrogate for the exact solution can be used in its place. Two common surrogates are the Richardson extrapolation, discussed in Appendix Section A.2, and the numerical solution on a much finer grid. The surrogate solution must be considerably more accurate than the solutions on either grid-1 or grid-2. Reference 18 discusses the inaccuracies that will occur if equation A4 is applied to a sequence of grids in which the surrogate is the solution on the finest grid of that sequence.

If neither the exact solution nor a suitable surrogate solution is available, the error model can be evaluated by fitting the error model through three grids. Fitting equation A2 to data from three grids, $i = 0, 1$ and 2, and taking the ratio of the difference between pairs of equations gives

$$\frac{\epsilon(h_2) - \epsilon(h_1)}{\epsilon(h_1) - \epsilon(h_0)} \equiv \frac{U(h_2) - U(h_1)}{U(h_1) - U(h_0)} = \left(\frac{h_1}{h_0}\right)^{\sigma} \left(\frac{(h_2/h_1)^{\sigma} - 1}{(h_1/h_0)^{\sigma} - 1}\right). \tag{A5}$$

If $h2/h1 = h1/h0$, the above equation reduces to

$$\frac{U(h_2) - U(h_1)}{U(h_1) - U(h_0)} = \left(\frac{h_1}{h_0}\right)^{\sigma}, \tag{A6}$$

and σ is given by

$$\sigma = \log\left(\frac{U(h_2) - U(h_1)}{U(h_1) - U(h_0)}\right) / \log\left(\frac{h_1}{h_0}\right). \tag{A7}$$

If $h2/h1 \neq h1/h0$, equation A5 can be solved iteratively for σ using a Newton iteration. Alternately, equation A5 can be recast into a form suitable for a simple fixed point iteration as follows:

$$\begin{aligned} &\sigma^{n+1} = \log\left(\tfrac{U(h_2)-U(h_1)}{U(h_1)-U(h_0)}\right) / \log\left(\tfrac{h_1}{h_0}\right) - P(\sigma^n) \\ &P(\sigma) = \log\left(\tfrac{(h_2/h_1)^\sigma - 1}{(h_1/h_0)^\sigma - 1}\right) / \log\left(\tfrac{h_1}{h_0}\right) \\ &\text{starting with } P(\sigma^0) \equiv 0. \end{aligned} \tag{A8}$$

With σ known, α can be determined from the difference between equation A2 on any two grids, and a fit of U_e can be determined from the ratio of equation A2 on any two grids. It is worth noting, and shown in Appendix Section A.2, that computing U_e in this way is equivalent to evaluating the Richardson extrapolation using the convergence rate given by the three-grid fit.

The similarity between equations A4 and A7 is not a coincidence. In the asymptotic regime in which $\sigma \approx p$, the difference between the solutions on two grids can be rewritten as follows:

$$\begin{aligned} U(h_2) - U(h_1) &= \alpha h_2^p (1 - (h_1/h_2)^p) \\ &= \epsilon(h_2)(1 - (h_1/h_2)^p) \\ &= \epsilon(h_2) S(p, h_2/h_1)^{-1} \end{aligned} \tag{A9}$$

in which $S(p, h_2/h_1)$ defines the scaling function used in this work. Thus, for a uniform grid refinement within the asymptotic regime

$$\frac{\epsilon(h_2) - \epsilon(h_1)}{\epsilon(h_1) - \epsilon(h_0)} \approx \frac{\epsilon(h_2)}{\epsilon(h_1)} \approx \frac{\epsilon(h_1)}{\epsilon(h_0)}. \tag{A10}$$

The above formulas, equations A1 – A9, are valid for *any* two or three grids within the asymptotic regime and with *any* grid ordering. Without loss of generality, the body of this work and the remaining Appendix Sections adopt the convention that $h_0 < h_1 < ... < h_n < h_{n+1}$. Equations A3 and A5 will be referred to as the 2-grid and 3-grid formulas, respectively. It is worth noting that the simple error model, equation A1, is a monotone equation, and any attempt to fit it to a nonmonotone data set is problematic. This issue is discussed further in the next Appendix Section. However, equations A3 and A5 and formulas derived from them are made valid, although not accurate, by replacing the left-hand side of each equation with its absolute value. Further, as a practical matter, the numerator and denominator of the left-hand sides must be bounded away from zero to avoid log(0) and division by zero.

The above formulas are precise only in the limit as the grid size goes to zero. For any two or three particular grids, the formulas represent curve fits that only approximate the asymptotic character of the data. In recognition of this fact, this work

denotes estimates of the error with the Δ symbol and defines particular estimates as $\Delta_{r,i} = (U(h_i) - U_r)$ and $\Delta_{h,i} = S(p, R_i)(U(h_i) - U(h_{i-1}))$ in which subscript $(.)_r$ denotes the Richardson extrapolation, and R_i denotes the ratio of grid sizes (h_i/h_{i-1}).

A.1 Oscillatory Convergence

As pointed out above, the error model is a monotone function; however, data exhibiting an oscillatory convergence pattern is not unusual. Figure A1 illustrates two instances of oscillatory convergence produced by the FUN3D code. A pattern of oscillatory convergence is not necessarily a bad characteristic for a CFD method to possess, as the error of a method that converges in an oscillatory pattern is often lower than that of a monotonically converging method. The effect of the oscillatory data on the convergence rate computation depends on the character of the oscillation and on the formula used (2-grid or 3-grid formula). Although the FUN3D lift coefficient is oscillatory, the two-grid formula can be applied without modification because all the data lies below the Richardson extrapolation of the FUN3D data. However, the error estimate of the three-grid formula, Δ_h, will change sign at each extrema. For C_{d_v}, shown in figure A1b, the oscillatory data will induce a single sign change into both Δ_h and Δ_r error estimates but at different locations.

Reference 13 provides a modification to the convergence rate computation that treats the oscillatory case, but it has a number of unsatisfying characteristics. The modification applies to the three-grid formulation and is based on switching the sign of the error model for one of the three equations. In particular, the equations

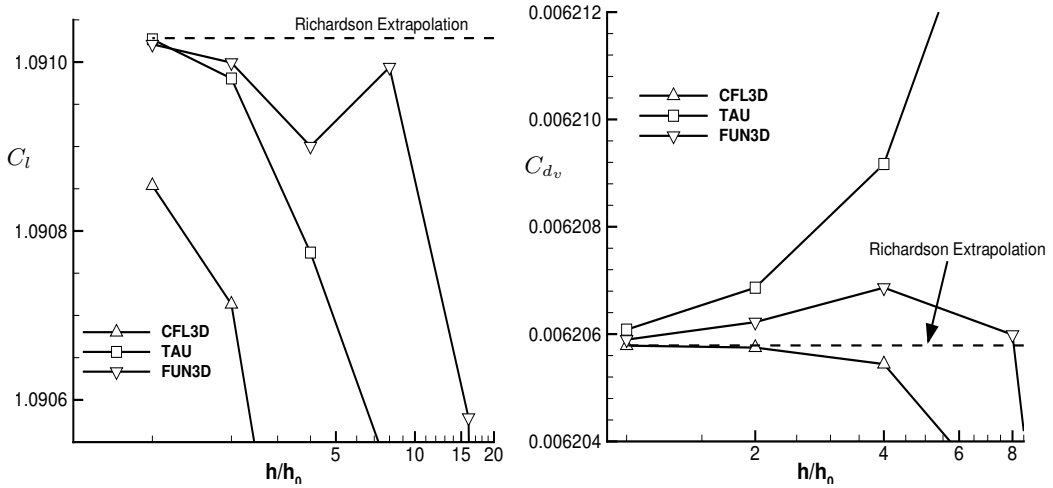

(a) C_l (b) C_{d_v}

Figure A1. Examples of oscillatory convergence. Dashed line is the Richardson extrapolation of the FUN3D data.

associated with the three grids are written as

$$\begin{aligned} \epsilon(h_2) &\equiv U(h_2) - Ue = \alpha h_2^\sigma \\ \epsilon(h_1) &\equiv U(h_1) - Ue = s\alpha h_1^\sigma \\ \epsilon(h_0) &\equiv U(h_0) - Ue = \alpha h_0^\sigma \end{aligned} \tag{A11}$$

in which $s = -1$ if the data on the three grids is oscillatory, otherwise $s = 1$ resulting in the usual three-grid formulation. This modification is equivalent to assuming that the exact solution lies within the local bounds of the oscillation, and that the basic error model is replaced with its absolute value:

$$\begin{aligned} \epsilon(h) &\equiv |U(h) - U_e| = \alpha h^\sigma \\ \text{and thus,} \quad U(h) - U_e &= \pm\alpha h^\sigma. \end{aligned} \tag{A12}$$

Carrying through the algebra from equation A11 gives:

$$\begin{aligned} \frac{\epsilon(h_2)-\epsilon(h_1)}{\epsilon(h_1)-\epsilon(h_0)} \equiv \quad \frac{U(h_2)-U(h_1)}{U(h_1)-U(h_0)} &= \left(\frac{h_1}{h_0}\right)^\sigma \left(\frac{(h_2/h_1)^\sigma - s}{s(h_1/h_0)^\sigma - 1}\right) \\ \frac{U(h_2)-U(h_1)}{U(h_1)-U(h_0)} &= \left(\frac{h_1}{h_0}\right)^\sigma \left(\frac{(h_2/h_1)^\sigma - s}{(h_1/h_0)^\sigma - s^{-1}}\right) \frac{1}{s} \\ s\left(\frac{U(h_2)-U(h_1)}{U(h_1)-U(h_0)}\right) &= \left(\frac{h_1}{h_0}\right)^\sigma \left(\frac{(h_2/h_1)^\sigma - s}{(h_1/h_0)^\sigma - s}\right) \\ \left|\frac{U(h_2)-U(h_1)}{U(h_1)-U(h_0)}\right| &= \left(\frac{h_1}{h_0}\right)^\sigma \left(\frac{(h_2/h_1)^\sigma - s}{(h_1/h_0)^\sigma - s}\right) \end{aligned} \tag{A13}$$

(Note: $s = \pm 1$ therefore $s^{-1} = s$).

The modification provides a justification for taking the absolute value of the ratio of the error estimates. However, it also introduces additional complexity associated with determining the sign of s that, as will be shown, does not improve the accuracy or validity of the computed convergence rate. Further if $h_2/h_1 = h_1/h_0$, the additional complexity falls out of the equation and the result is only that of taking the absolute value of the ratios of the error estimates.

Figure A2 illustrates the convergence rates of an analytic error function computed by applying the full correction described in reference 13, and shown above in equation A13, with that of only taking the absolute value of the ratio of error estimates. The analytic error function is constructed from an approximate fit to the FUN3D C_l data shown in figure A1a and is given by:

$$C_l = 1.091023 + 2 \cdot 10^{-5}(h/h0)^2 \left[1 - \frac{h/h0)}{5} + \left(\frac{h/h0)}{10}\right)^2 + \left(\frac{h/h0)}{40}\right)^3\right]. \tag{A14}$$

The analytic error function allows the convergence rates to be computed for any value of h/h_0 using any grid refinement ratios desired. The results shown in figure A2 are computed assuming the grid spacing is increasing in a geometric manner as the grid is coarsened: $h_{n+1}/h_n = 1.2h_n/h_{n-1}$ with $h_n/h_{n-1} = 2$. The predictions using the two formulas for nonuniform refinement are identical whenever all three points are in a monotone region. Both formulations give similarly *inaccurate* results within the oscillatory region. Figure A2 contains two additional curves that provide some

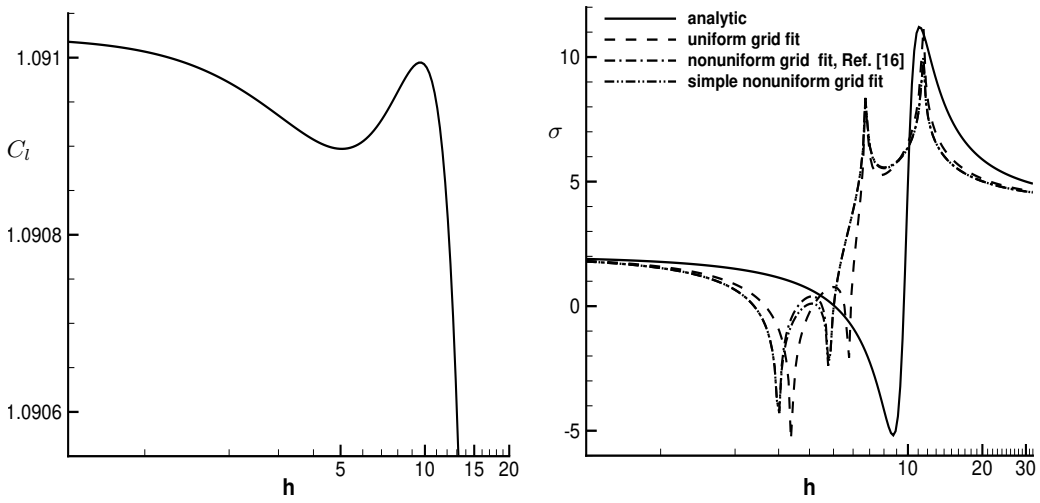

(a) Error function constructed from FUN3D C_l data. (b) Convergence rates, σ.

Figure A2. Error function constructed from FUN3D C_l data, and convergence rates for nonuniform refinement resulting from formulation of reference 13, from a simplified form that just takes the absolute values of arguments, and from uniform refinement and analytic formulations.

context. The dashed line is the convergence rate computed for a uniform refinement with $h_{n+1}/h_n = h_n/h_{n-1} = 2$, and the solid line is an analytic convergence rate derived as follows.

$$\begin{aligned} \text{Given} \qquad \epsilon(h) \equiv U(h) - U_e &= \alpha h^\sigma \\ \tfrac{\partial U(h)}{\partial h} &= \sigma \alpha h^{\sigma-1} \\ &= \sigma (U(h) - U_e)/h \\ \text{therefore} \qquad \sigma &= h \tfrac{\partial U(h)}{\partial h} / (U(h) - U_e), \end{aligned} \tag{A15}$$

in which U_e may be replaced with a surrogate value. All four formulations predict similarly large and small (negative) values of the computed convergence rate within the oscillatory region, although the spikes in the discrete forms would go to $\pm\infty$ if the computations were not bounded in some manner. All four formulations are simply indicating that a simple error model of the form αh^σ *cannot* be fit to a nonmonotone function with any degree of accuracy. The recommendation is to not try to fix the formulas, but to acknowledge that the formulas are indicating that the data are not exhibiting an asymptotic behavior in the oscillatory region, and that the computed convergence rate is invalid.

A.2 Richardson Extrapolation

The Richardson extrapolation (refs. 8,11) was developed as a means of estimating the asymptotic solution in the limit of the mesh size going to zero. It was arrived at by fitting the simple error model, A1, to data from two grids subject to the assumption

that the convergence rate is known. Replacing U_e with U_r in equation A1, to indicate that it is the result of a particular curve fit, and solving for U_r gives

$$\begin{aligned} U(h_2) - U_r(h_1) &= (U(h_1) - U_r(h_1))R^p \\ U_r(h_1)(R^p - 1) &= U(h_1)R^p - U(h_2) \\ U_r(h_1) &= (U(h_1)R^p - U(h_2))/(R^p - 1) \end{aligned} \tag{A16}$$

in which $R = h_2/h_1$. The method was only vaguely described in reference 8, however, the approach was applied to estimate the error of a string vibration problem and a two-dimensional plate vibration problem. The work also demonstrated that the Richardson extrapolation converged faster than the discrete solution. In reference 11, Richardson presented equation A16 and named the formula the "h^2-extrapolation" (when applied to a second-order discretization). Reference 11 also mentioned the possibility of extending the process to higher order obtaining a "h^4-extrapolation" using only three grids (when using central difference operators) but did not develop it further.

In references 8 and 11, the power p was always taken as the leading term of the discretization error. It is clear that using the convergence rate determined from a three-grid fit and evaluating equation A16 using any two of the three grids would result in the limiting value of the curve passing through the data from those three grids. While this provides a convenient formula for estimating U_e associated with the three-grid fit, which will be denoted as U_f, this value should be considered distinct from that of the Richardson extrapolation. The Richardson extrapolation should be viewed as an asymptotic expansion about the (unknown) exact solution, and as such, the expansion should use the theoretical order property of the discretization method. In the asymptotic regime, the two values should converge toward a common value in a similar manner. However, outside of the asymptotic regime, and particularly in an oscillatory region, the convergence rate predicted by the three-grid fit can vary widely with no relation to the asymptotic value, and an extrapolation or error estimation based on this computed σ will also vary widely and be suspect. Figures A3(a) and (b) present the convergence of U_r and U_f, and error estimates based on the surrogates U_r and U_f, respectively. The results are computed using the analytic model of the error given by equation A14. In the limit as the mesh size goes to zero, both U_r and U_f converge to the exact solution at a higher rate than that of the solution. It is now well known that the Richardson extrapolation is a (p+1)-order approximation to U_e, and this is readily shown simply by including higher-order truncation terms in the derivation. Near the upper limits of the asymptotic regime, the error in U_r is smooth while the error in U_f is much larger and erratic.

In figure A3(a), error estimates using either U_r or U_f as a surrogate converge to the exact error in the limit of the grid size going to zero; so either would be an accurate surrogate for U_e if the finest grid is sufficiently fine. Figure A3(b) presents the error estimate that would be obtained on the finest grid if h was the mesh size of the finest grid of a sequence (i.e., the figure depicts $U(h) - U_x(h)$ for $x = f$ or r, not $U(h) - U_x(h_0)$ for some small h_0). An estimate based on U_r would underpredict the error near the upper limits of the asymptotic regime, but the error estimates

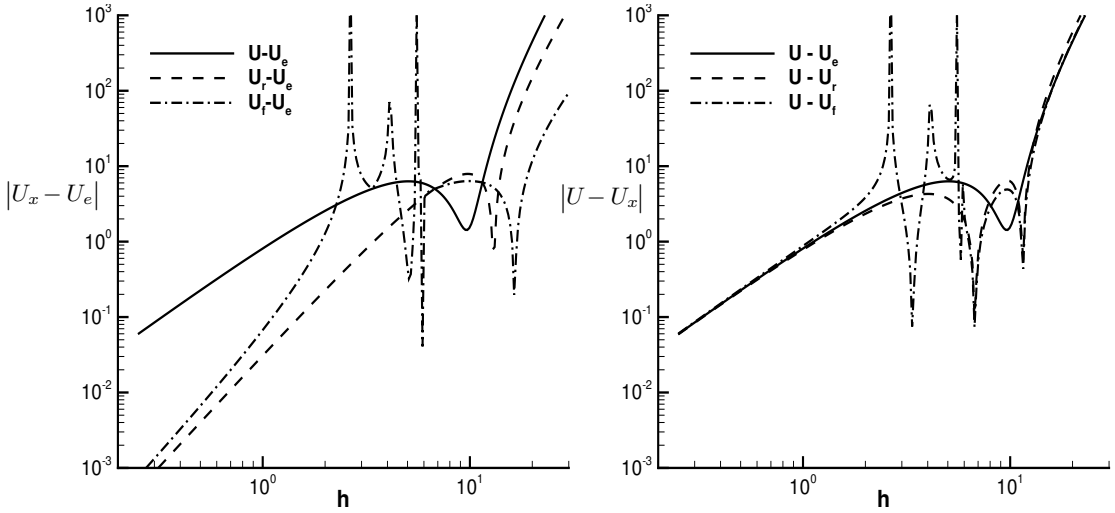

(a) Convergence of the Richardson extrapolation, $U_r - U_e$, and of the extrapolation from the three-grid fit, $U_f - U_e$, compared to the exact error, $U - U_e$.

(b) Error estimates using extrapolated values as a surrogate for the exact solution compared to the exact error.

Figure A3. Convergence of surrogate solutions as approximations of the exact solution, and of error estimates based on surrogates solutions for an error model constructed from FUN3D C_l data.

would be smooth. In contrast, error estimates based on U_f may either over- or underpredict the error by orders of magnitude depending on small changes in the size of the finest grid. This illustrates a risk associated with using any surrogate solution when it is not known if the finest grid is in the asymptotic regime, and that the risk is highest when U_f is used as a surrogate solution. Note that similar behavior could be expected for any method or property exhibiting nonmonotone convergence. It is recommended that an extrapolated surrogate solution be used *only* if it has been established that the data it is based on is within the asymptotic regime. Also, the Richardson extrapolation based on a known (or presumed) design order is preferred over an extrapolation based on a computed order (i.e., that from a three grid extrapolation).

A.3 High-order Extension to Richardson's Extrapolation

The Richardson extrapolation can be extended to higher order by fitting a high degree polynomial form of the error model through data from a larger sequence of grids. Such a fit is defined by solving set of the equations given by

$$U_i = U_{r_N,n} + \sum_{j=0}^{N-2} \alpha_j (h_i/h_n)^{p+j} \qquad \text{for grids in the set} \qquad n \le i < n+N \quad \text{(A17)}$$

in which p is the design order, and $U_{r_N,n}$ denotes the value in the limit of h going to zero. The procedure applies equally well to a uniform or a nonuniform grid

refinement sequence, and it also applies to monotone or oscillatory convergence data. The equation set can be represented in matrix form $\mathbf{U} = \mathbf{AR}$ in which $\mathbf{R} \equiv [U_{r_N,n}, \alpha_0, \alpha_1, \ldots, \alpha_{N-2}]$, $\mathbf{U} \equiv [U_n, U_{n+1}, \ldots, U_{n+N-1}]$, and the N by N matrix $\mathbf{A}$ is given by

$$a_{i,j} = \begin{cases} 1 & \text{for } j = 1 \\ (h_{n+i-1}/h_n)^{p+j-2} & \text{for } j > 1 \end{cases} \tag{A18}$$

The condition number of the matrix $\mathbf{A}$ grows rapidly with the degree of the fit. For a uniform grid refinement with a refinement ratio of R, the condition number is $O(R^{(n-1)(n+p-2)})$. However, the ill-conditioning of $\mathbf{A}$ can be eliminated by a diagonal scaling of the form $\hat{\mathbf{A}} \equiv \mathbf{DAD}$ in which $d_{i,i} = 1/\sqrt{a_{i,i}}$. The condition number of $\hat{\mathbf{A}}$ is $O(10^3)$ for a uniform refinement with $N = 14$.

The convergence of $U_{r_N,n}$ was presented in figure 6, in which the error was estimated as the difference between fits of different order as the grid was refined. Generally the convergence rate of $U_{r_N,n}$ is higher order than the solution itself. In contrast, it was difficult to even assess the error in the standard Richardson extrapolation.

The formula for the high-order Richardson extrapolation can be recast, as was shown in equation 7, to provide an estimate for the upper threshold of the asymptotic regime. Table 3 presented the threshold for the four force coefficients for each of the three CFD codes. Table A1 presents FUN3D data that examines in detail how the threshold converges as the order of the extrapolation increases. The table gives $S_k \hat{h}_k / h_0$ for curve fits of increasing order that include the finest grid. Except for the $k = 1$ terms of C_{d_p}, all terms are converging as the degree of the fit is increased. The smaller values that determine the threshold of the asymptotic regime converge well.

C_l					
k	N=3	N=4	N=5	N=6	N=7
1	14.8	0.732	-0.224	-0.465	-0.553
2		-2.34	1.12	1.52	1.61
3			-3.11	-3.35	-3.32
4				6.79	6.10
5					-11.1
C_d					
k	N=3	N=4	N=5	N=6	N=7
1	81.4	201	-314	-115	-84.3
2		29.93	18.3	14.9	13.6
3			-19.7	-15.2	-13.6
4				21.0	17.5
5					-25.7
C_{d_p}					
k	N=3	N=4	N=5	N=6	N=7
1	32.7	35.4	46.8	61.9	76.5
2		53.99	23.0	17.5	15.6
3			-21.1	-15.9	-14.1
4				21.5	17.8
5					-26.0
C_{d_v}					
k	N=3	N=4	N=5	N=6	N=7
1	-6.93	-5.54	-5.11	-4.94	-4.86
2		11.72	9.25	8.44	8.09
3			-14.7	-12.0	-11.1
4				18.5	15.7
5					-24.1

Table A1. Convergence of $S_k\hat{h}_k/h_0$ for FUN3D as degree of fit N is increased.

REPORT DOCUMENTATION PAGE	Form Approved OMB No. 0704–0188

The public reporting burden for this collection of information is estimated to average 1 hour per response, including the time for reviewing instructions, searching existing data sources, gathering and maintaining the data needed, and completing and reviewing the collection of information. Send comments regarding this burden estimate or any other aspect of this collection of information, including suggestions for reducing this burden, to Department of Defense, Washington Headquarters Services, Directorate for Information Operations and Reports (0704-0188), 1215 Jefferson Davis Highway, Suite 1204, Arlington, VA 22202-4302. Respondents should be aware that notwithstanding any other provision of law, no person shall be subject to any penalty for failing to comply with a collection of information if it does not display a currently valid OMB control number.
PLEASE DO NOT RETURN YOUR FORM TO THE ABOVE ADDRESS.

1. REPORT DATE *(DD-MM-YYYY)*	2. REPORT TYPE	3. DATES COVERED *(From - To)*
01-10-2018	Technical Memorandum	

4. TITLE AND SUBTITLE

Convergence Analysis of Turbulent Flow Solutions

5a. CONTRACT NUMBER

5b. GRANT NUMBER

5c. PROGRAM ELEMENT NUMBER

6. AUTHOR(S)
Harold L. Atkins

5d. PROJECT NUMBER

5e. TASK NUMBER

5f. WORK UNIT NUMBER
109492.02.07.01.01

7. PERFORMING ORGANIZATION NAME(S) AND ADDRESS(ES)
NASA NASA Langley Research Center
Hampton VA 23681-2199

8. PERFORMING ORGANIZATION REPORT NUMBER
L–20961

9. SPONSORING/MONITORING AGENCY NAME(S) AND ADDRESS(ES)
National Aeronautics and Space Administration
Washington, DC 20546-0001

10. SPONSOR/MONITOR'S ACRONYM(S)
NASA

11. SPONSOR/MONITOR'S REPORT NUMBER(S)
NASA/TM–2018–220106

12. DISTRIBUTION/AVAILABILITY STATEMENT
Unclassified-Unlimited
Subject Category 02
Availability: NASA STI Program (757) 864-9658

13. SUPPLEMENTARY NOTES
An electronic version can be found at http://ntrs.nasa.gov.

14. ABSTRACT Data from the "Turbulence Modeling Resource" website for turbulent flow over an NACA-0012 airfoil is analyzed to determine the convergence behavior of three second-order CFD codes: CFL3D, FUN3D, and TAU. The convergence of both integrated properties and pointwise data are examined. Several different methods for estimating errors and computing convergence rates are compared. A high-order extension to the Richardson extrapolation is developed that improves the accuracy of the mesh limit values and provides a quantitative estimate of the threshold of the asymptotic regime. The coefficient of total drag exhibits second-order convergence for all three codes, and convergence is monotone over a sequence of 7 grids. Other force coefficients are not so well behaved. The convergence rates of the viscous component of drag on the three finest grids ranges from ≈ 3.0 for CFL3D to ≈ 1.0 for FUN3D. The three codes are converging to similar but not identical solutions. The largest differences between the codes are in the coefficient of lift for which the difference between CFL3D and FUN3D is greater than 10^{-4}. The best agreement occurs in the viscous component of drag, which is the only force component for which all three codes are converging towards each other at a rate of second-order. The agreement between the two unstructured grid codes is good with all properties except lift converging towards common values at a rate of second-order. No one code was universally better than the other. The TAU code has the lowest error in total drag, FUN3D has the lowest error in lift, and CFL3D has the lowest error in the viscous component of drag.

15. SUBJECT TERMS
Computational fluid dynamics,Aerodynamics, Error Assessment, Convergence Assessment

16. SECURITY CLASSIFICATION OF:			17. LIMITATION OF ABSTRACT	18. NUMBER OF PAGES	19a. NAME OF RESPONSIBLE PERSON
a. REPORT	b. ABSTRACT	c. THIS PAGE			STI Information Desk (help@sti.nasa.gov)
U	U	U	UU	44	19b. TELEPHONE NUMBER *(Include area code)* (757) 864-9658